To the Graduate Council:

I am submitting herewith a thesis written by Hiromoto Kuroda entitled "Aerodynamic Interaction of Heat Transfer with Steady Transonic Flow." I recommend that it be accepted in partial fulfillment of the requirements for the degree of Master of Science, with a major in Engineering Science.

Mitsuru Kurosaka, Major Professor

We have read this thesis
and recommend its acceptance:

Accepted for the Council:

Vice Chancellor
Graduate Studies and Research

AERODYNAMIC INTERACTION OF HEAT TRANSFER WITH STEADY TRANSONIC FLOW

A Thesis

Presented for the

Master of Science

Degree

The University of Tennessee, Knoxville

Hiromoto Kuroda

June 1981

3051722

ACKNOWLEDGMENTS

The author's deepest thanks are extended to his advisor, Dr. Mitsuru Kurosaka, for invaluable guidance and support during the course of this investigation. Special thanks are also extended to Dr. Robert L. Young and Dr. Jain-Ming Wu for their many constructive criticisms and suggestions and the knowledge they tried to impart to the author as members of his examination committee.

Acknowledgment is also expressed to Dr. Hsian P. Chou for helping with the experiments and the computational work.

The author wishes to thank Mr. Richard Ray for his technical assistance and operating the wind tunnel, and Mr. James Goodman for helping to set up the combustor.

The work reported herein was supported by NASA Lewis Research Center, Cleveland, Ohio, Grant No. 3487. This grant was monitored by Dr. R. Siegel.

The author wishes to extend sincere thanks to Ms. June Jarrell for her excellent typing of the final manuscript of this thesis.

Finally, the author would like to dedicate this thesis to his wife, Yasuko, for her moral support and for taking care of their two young sons, Akihiro and Nobuhiro.

ABSTRACT

This thesis is concerned with the effect of heat transfer on steady transonic flow in a two-dimensional, convergent-divergent duct. The problem was studied by means of experiments in a combustion tunnel.

An experimental investigation to determine the shock position and sonic line was carried out at total pressures ranging between 4 and 20 psig, total temperatures between 40 and 1000°F and wall temperatures between 50 and 900°F. Detailed duct wall pressures and shock positions were obtained for various expansion ratios and wall-to-fluid temperature ratios. The two-dimensionality of the duct flow was verified by wall pressure measurements. In addition, the fact that the flow was turbulent was verified.

For the experimental conditions investigated, it was confirmed that the change of the sonic line due to the effect of the heat transfer was small. However, the displacement thickness downstream of the shock became markedly thinner as the duct walls were cooled. Thus the position of the shock was shifted by wall cooling. The extent of the shock movement in the present experiment was of the same order as the throat height for the expansion ratio p_e/p_t of about 0.5 and wall-to-fluid temperature ratio T_w/T_t of approximately 0.5.

TABLE OF CONTENTS

CHAPTER		PAGE
I.	INTRODUCTION	1
II.	COMBUSTION TUNNEL AND ITS TEST SECTION	8
	1. Combustor	8
	2. Diffuser and Settling Chamber	11
	3. Test Section (Convergent-Divergent Duct)	14
III.	INSTRUMENTATION	18
	1. Temperature Measurement	18
	2. Pressure Measurement	18
	3. Schlieren System	19
	4. Boundary Layer Pressure Probe	21
IV.	EXPERIMENTAL RESULTS	23
	1. Experiments for Hot Run	25
	2. Experiments for Cold Run	39
V.	DISCUSSION OF EXPERIMENTAL RESULTS	45
	1. Sonic Location	45
	2. Shape of Boundary Layer Profiles	46
	3. Schlieren Observation	52
	4. Boundary Layer Thickness	52
	5. Shift of Normal Shock	58
VI.	CONCLUSIONS	62
LIST OF REFERENCES		64
APPENDICES		69
APPENDIX A.	RELATIONSHIP BETWEEN HEAT TRANSFER AND SHIFT OF SONIC LINE	70
APPENDIX B.	ACCELERATION PARAMETER	72
APPENDIX C.	WALL HEAT FLUX FROM TOP AND BOTTOM WALLS	74
APPENDIX D.	DATA REDUCTION WITHIN BOUNDARY LAYER	76
APPENDIX E.	PRESSURE RATIO AND MACH NUMBER UPSTREAM OF SHOCK	80

CHAPTER PAGE

APPENDIX F. AREA RATIO DOWNSTREAM OF SHOCK 83

VITA. 85

LIST OF FIGURES

FIGURE		PAGE
1.	Cooling Blade (Conway's Turbine Blade)	2
2.	Construction of Film Cooled Blades	3
3.	Flow Near Trailing Edge of Turbine Nozzle.	4
4.	Test Rig Layout.	9
5.	View of Test Facility.	10
6.	Contour of Two-Dimensional Convergent-Divergent Duct	15
7.	Comparison of Contours	16
8.	Pressure Taps on Top and Bottom Walls.	20
9.	Total Pressure Probe	22
10.	Pressure Distribution to Confirm Two-Dimensionality (Cold Run).	24
11.	Mean Pressure Distribution in Test Duct.	26
12.	Shock Location (Hot Run); $p_e/p_t = 0.520$, $p_e/p_t = 0.525$	27
13.	Shock Location (Hot Run); $p_e/p_t = 0.597$, $p_e/p_t = 0.595$	28
14.	Shock Location (Hot Run); $p_e/p_t = 0.663$, $p_e/p_t = 0.669$	29
15.	Shock Location (Hot Run); $p_e/p_t = 0.800$	30
16.	Relationship of Shock Location with Expansion Ratio and Temperature Ratio (Hot Run).	33
17.	Pressure Distribution and Displacement Thickness (Hot Run); $p_e/p_t = .520$, $p_e/p_t = .525$. . .	35
18.	Pressure Distribution and Displacement Thickness (Hot Run); $p_e/p_t = .597$, $p_e/p_t = .595$. . .	36

FIGURE PAGE

19. Pressure Distribution and Displacement Thickness (Hot Run); $p_e/p_t = .663$, $p_e/p_t = .669$. . . 37

20. Pressure Distribution and Displacement Thickness (Hot Run). 38

21. Shock Location (Hot Run); $p_e/p_t = 0.648$, $p_e/p_t = 0.653$ 40

22. Pressure Distribution (Cold Run) 42

23. Relationship of Shock Position with Expansion Ratio and Temperature Ratio (Cold Run) 43

24. Acceleration Parameter at Throat 47

25. Velocity Distribution at x = -1.0 and 2.3 Inches (Cold Run). 49

26. Velocity and Temperature Distribution Downstream of Shock (x = 3.6 Inches) (Hot Run) 51

27. Bifurcated Oblique Shock Angle 53

28. Displacement Thickness Downstream of Shock (Hot Run). 55

29. Effect of Cooling upon Boundary Layer Thickness Downstream of Shock. 60

LIST OF SYMBOLS

A	area of cross-section
a	acoustic speed
c_p	specific heat at constant pressure
G	mass flow rate
H	Form factor ($= \delta^*/\theta$)
h	height of test section in inches
K	acceleration parameter $\left(= \frac{\mu_e}{\rho_e u_e^2} \frac{d u_e}{dx} \right)$
k	coefficient of thermal conductivity
M	Mach number ($= u/a$)
p	pressure
Pr	Prandtl number ($= c_p \mu/k$)
Q	heat transfer rate per unit mass
q	heat flux per unit area
R	Gas constant
Re	Reynolds number
r	recovery factor
T	temperature
u	stream velocity in x-direction
u_τ	frictional velocity ($= \sqrt{\tau_w/\rho_w}$)
x	coordinate in streamwise direction ($x = 0$ at throat)
y	coordinate normal to wall

α divergent half-angle in Figure 7

β separation angle in Figure 27

γ ratio of specific heats

δ^* displacement thickness $\left(= \int_0^{h/2} \left(1 - \frac{\rho u}{\rho_e u_e} \right) dy \right)$

θ momentum thickness $\left(= \int_0^{h/2} \frac{\rho u}{\rho_e u_e} \left(1 - \frac{u}{u_e} \right) dy \right)$

μ dynamic viscosity of fluid

ρ density of fluid

τ shearing stress

ϕ oblique shock angle

Subscripts

b inside of boundary layer

co combustor

e edge of boundary layer, or exhaust in p_e

s shock, or separation in p_s

st settling chamber

t stagnation state

th throat

w on the wall

1 just upstream of shock

2 just downstream of shock

CHAPTER I

INTRODUCTION

Gas turbine engine performance has been continually improved by the steady advancement of turbine technologies, which has permitted the operating temperature and pressure to become considerably higher. The design and subsequent performance of air-cooled blades proved to play the critical roles in attempts to achieve desired turbine efficiency at the current high level of operating temperatures and pressures. These improvements led to the turbine blades operating successfully at high stage loading and Mach number.

Figure 1 shows a typical impingement cooling blade which is installed in the Conway engines. Also, the F-404 turbofan engines are one of the recent engines with high- and low-pressure turbines, each consisting of only a single stage using highly loaded, air-cooled blades. These blades use film cooling similar to that shown in Figure 2.

The high-loading turbine blades usually operate in transonic flow regime and the blade exit velocity is supersonic. Therefore, it may be expected that such losses as those due to shocks are necessarily increased. Figure 3 shows the pattern of shock waves and streamlines near the trailing edge of blades at different expansion ratio. The accurate prediction of sonic line and shock pattern in

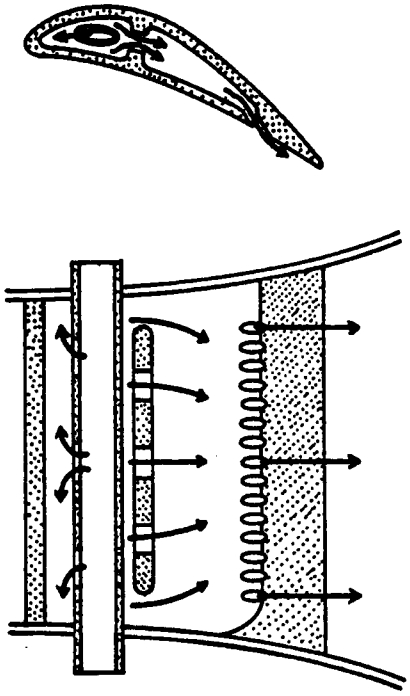


Figure 1. Cooling Blade (Conway's Turbine Blade).

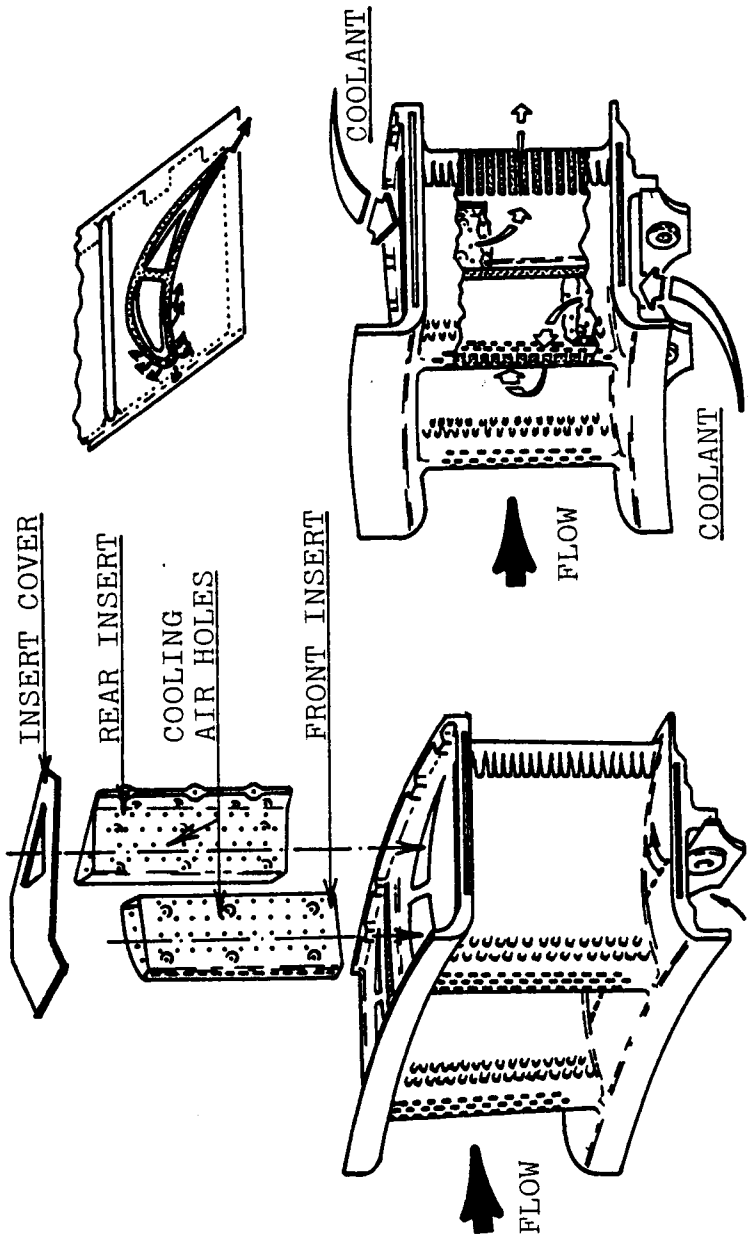
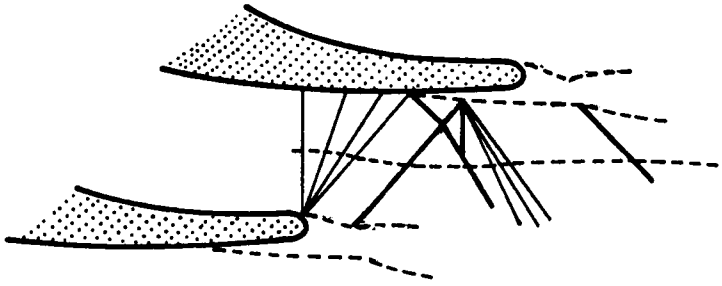
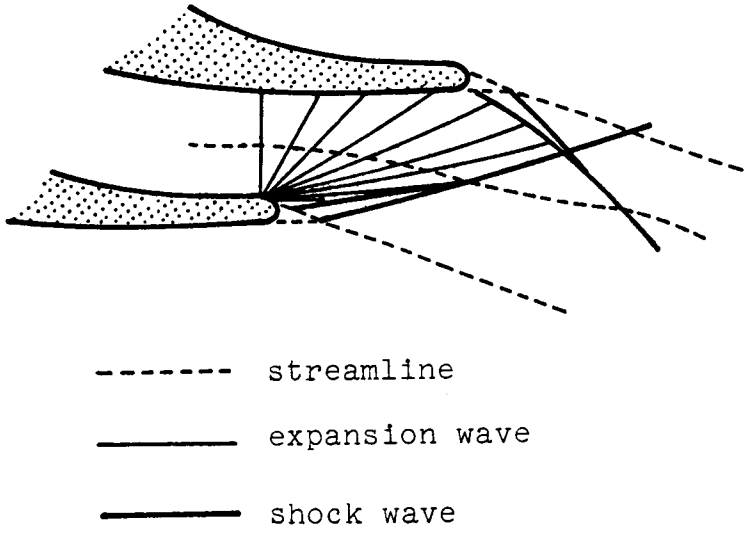


Figure 2. Construction of Film Cooled Blades.



(a) Shock and Streamline for High Expansion Ratio



(b) Shock and Streamline for Low Expansion Ratio

Figure 3. Flow Near Trailing Edge of Turbine Nozzle.

design is obviously important for the estimation of shock losses and stage loadings.

In the current design practice, the sonic line and shock patterns are usually predicted by the blade-to-blade or cascade flow analysis. McDonald [1][1] predicted steady transonic flow through two-dimensional gas turbine cascades using a time-dependent formulation of the equation of motion. Delaney and Kavanaugh [2] calculated the flow in axial-flow cascades using the second order time-dependent method, and Ives and Liutermoza [3] solved two-dimensional cascades flow using conformal mapping and the relaxation method. However, none of the above analyses, being restricted to inviscid flow, take the effect of boundary layer into account. The effect of boundary layer upon the inviscid flow is discussed by Gliebe [4]. Unfortunately, the boundary-layer calculation method adopted therein is restricted to a thermally insulated wall without any mass injection.

In a cooled turbine passage, as shown in Figure 2, the heat and mass transfer process caused by blade cooling and coolant injection may significantly interfere with the main steady flow field and markedly alter the sensitive transonic flow regime (on the contrary, for the subsonic

---

[1]Numbers in brackets refer to similarly-numbered references in the List of References.

flow, such effect is expected to be small as postulated to be so by Hartsel [5] and collaborated, in an indirect manner, from a series of efficiency data [6-10]). Even in the inviscid core region outside of boundary layers, a simplified, one-dimensional analysis [11] displays the well-known important effect of heat and mass transfer on the transonic flow; the effect may be as influential as a change in the cross-section area. In the turbine transonic flow, the response of the boundary layer to the effect of heat and mass transfer may become amplified to a sizeable extent.

In spite of the expected importance of the interactive effect of heat and mass transfer on the transonic turbine stage, to the best knowledge of the present author there is only the work of Studerus [12], who examined the effect of heat and mass transfer due to coolant injection into the mainstream. He conducted his study in the framework of inviscid flow by modifying the normal component of velocity on the airfoil surface to non-zero values. Therefore, not only the effect of heat transfer but also the behavioral change of the boundary layer on the transonic flow and its resulting influence upon the pressure distributions are outside the scope of his investigation.

The present work is the first attempt to clarify the above and its specific aim is to study the interactive effect of heat transfer--this effect only--on the transonic

flow field; the effect of the mass transfer is relegated to further work. To achieve the objective in a simplified environment devoid of geometrical complexity, a convergent-divergent duct representative of a turbine passage has been chosen as a test section and the effect of cooling wall upon the steady transonic flow field has been investigated experimentally. This study has been presented in a preliminary form in Reference [13].

CHAPTER II

COMBUSTION TUNNEL AND ITS TEST SECTION

The present experiment has been conducted in the combustion wind tunnel at The University of Tennessee Space Institute. The configuration is shown in Figures 4 and 5. The tunnel comprises three major sections: (1) combustor, (2) diffuser and settling chamber, and (3) test section. These are explained in detail below.

1. Combustor

A modified can-type combustor of the J-79 jet engine was adopted for the present tunnel. Since the flow rate of the tunnel is less than the design condition of the J-79 engine, some secondary air holes in the combustor liner were blocked to meet our test need. Kerosene is used as the fuel and it is stored in a 50-gallon reservoir. During the test, a 1/2 HP electrically-driven pump maintains the fuel pressure at constant-pressure setting of the valve before it is fed into the fuel control unit. In the present work, the setting was 45 psig. The pneumatic control valve in the fuel line is used to regulate the fuel flow rate required by the combustor. The operation range of the pneumatic regulator requires pressure variations up to 15 psig between fully-closed and fully-open positions. Subsequently, fuel is injected into the combustor by a fuel nozzle with a diameter of 0.075 inches.

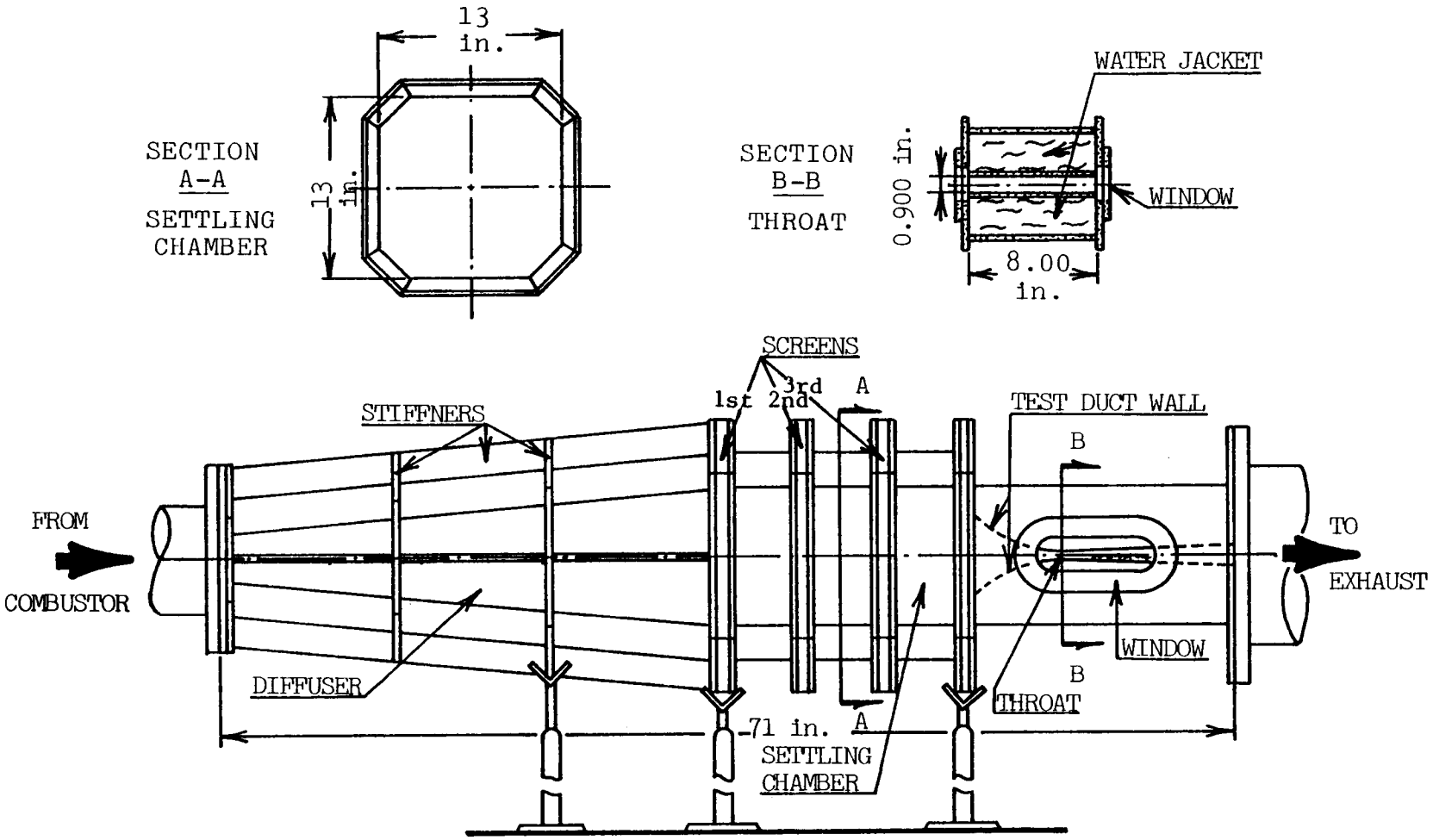


Figure 4. Test Rig Layout.

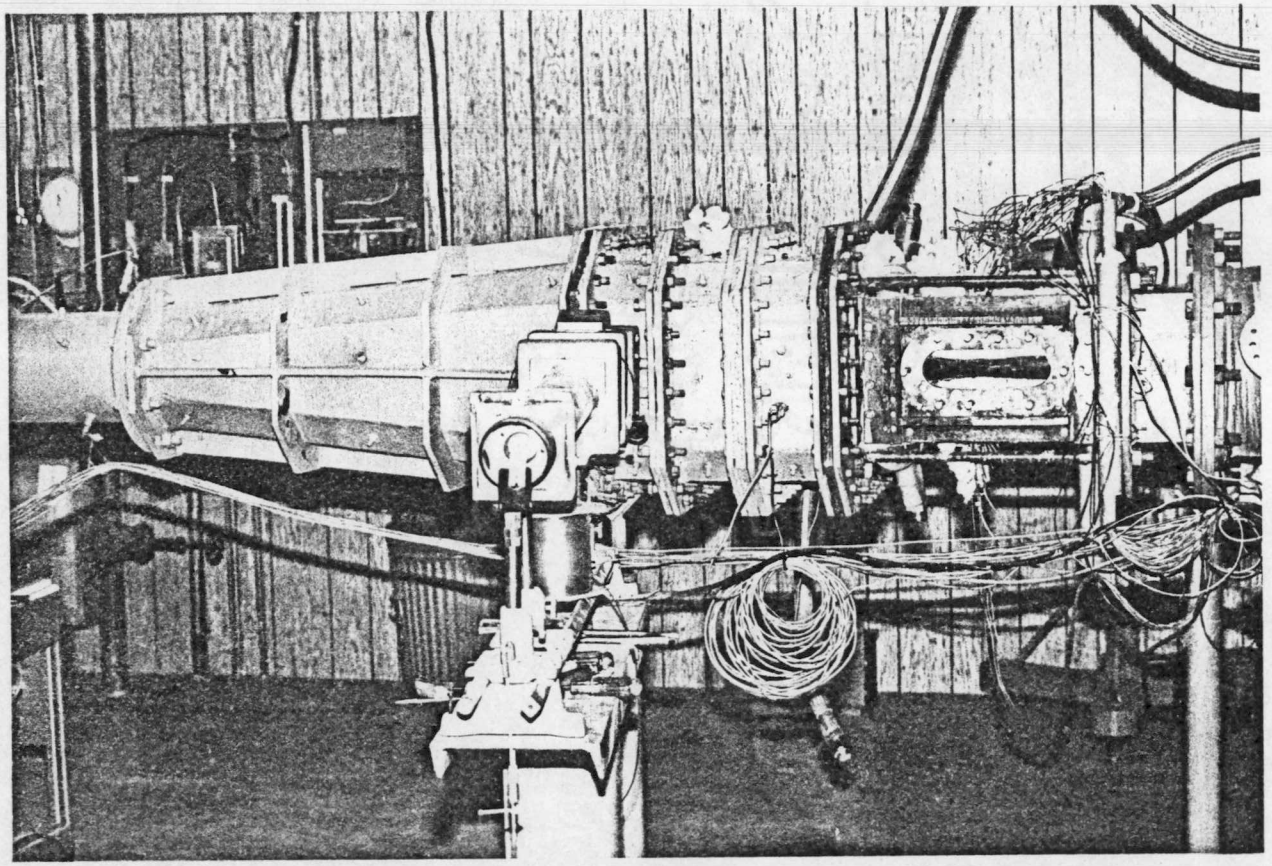


Figure 5. View of Test Facility.

The fuel spray in the combustor is initially ignited by a premixed propane/air flame; a furnace-type igniter is provided with a set of two automobile spark plugs. Remotely-controlled solenoid valves regulate the mixture of propane and air with an appropriate pressure such that the flame is firmly established. After the kerosene is completely ignited, the flow of propane/air mixture is shut off externally. The normal operating conditions of the combustor during the test are listed in Table 1.

2. Diffuser and Settling Chamber

The air leaves the combustor at a typical temperature of around 1300°R (measured by Chromel-Alumel thermocouples) and with high turbulent intensity resulting from combustion. An octagonally cross-sectioned diffuser with half-angle equal to five degrees is installed immediately after the combustor to achieve the following two purposes: (a) to convert the flow pattern gradually from the circular cross-section of the combustor into a subsequent rectangular one of the test section, and (b) to recover the flow static pressure.

Downstream of the diffuser, it is connected to a settling chamber in which three stainless steel wire screens, five inches apart, are installed in order to further reduce the turbulence level. The specifications of each of the wire screens are shown in Table 2.

TABLE 1

CONDITIONS OF COMBUSTOR

A_{co} $in.^2$	G lbm/sec	$T_{t,co}$ °R	$p_{t,co}$ psia
38.5	1-6.3	500-1500	18-40

TABLE 2

DESCRIPTIONS OF SCREEN (STAINLESS STEEL)

Position	Mesh	Wire Dia. in.	Opening %	Direction of Wire
First	2x2	0.105	62.4	Horizontal and Vertical
Second	2x2	0.105	62.4	Diagonal
Third	5x5	0.072	41.0	Horizontal and Vertical

It is believed that the diffuser and settling chamber designs in the present rig can achieve the better flow quality of low turbulence as well as near reservoir condition before the flow enters the test section.

The inner walls of the diffuser and settling chamber are coated with aluminum-oxide based refractory material of one-inch thickness to protect the metal wall and its stiffeners thermally. No heat damage has been detected during the entire tests.

3. Test Section (Convergent-Divergent Duct)

A convergent-divergent duct with as much two-dimensional flow as possible was selected for the test section to simulate approximately the area change in a typical transonic turbine flow passage between stator blades. The contour of the convergent-divergent duct is shown in Figure 6, and Figure 7 shows the comparison of the contour of the present test section with transonic and supersonic cascades. The present test section has a throat of 0.9-inch height and 8.0-inch width. It consists of a convergent section with a constant radius of curvature of 10.0 inches and the divergent section with 2.62° half-angle straight walls. The downstream end of the divergent duct is connected to the back pressure control flaps. The contoured walls are made of copper of 1/4-inch thickness and are either cooled by water circulating through the water jacket or heated by 3kw oven-type electric heaters.

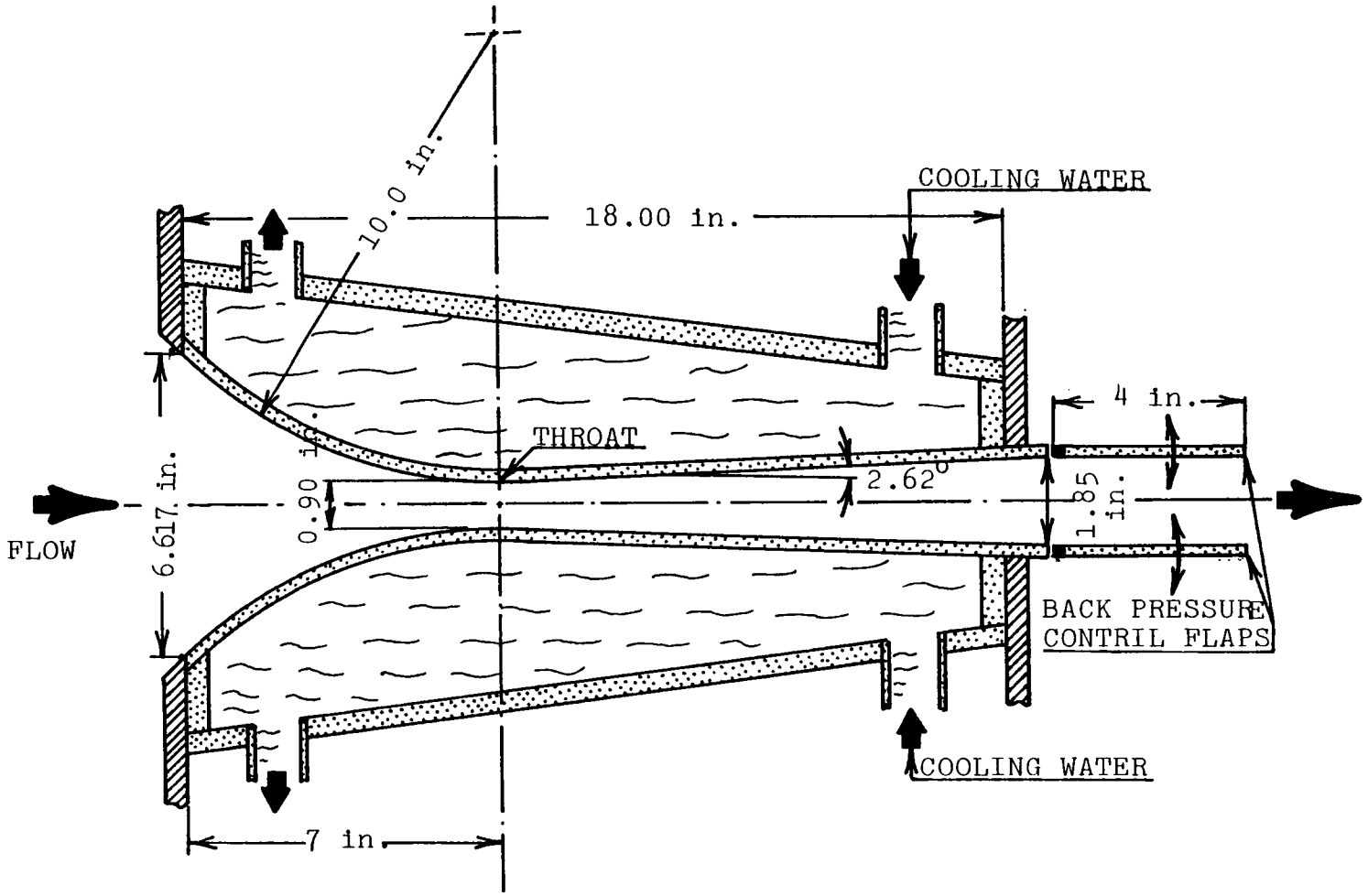


Figure 6. Contour of Two-Dimensional Convergent-Divergent Duct.

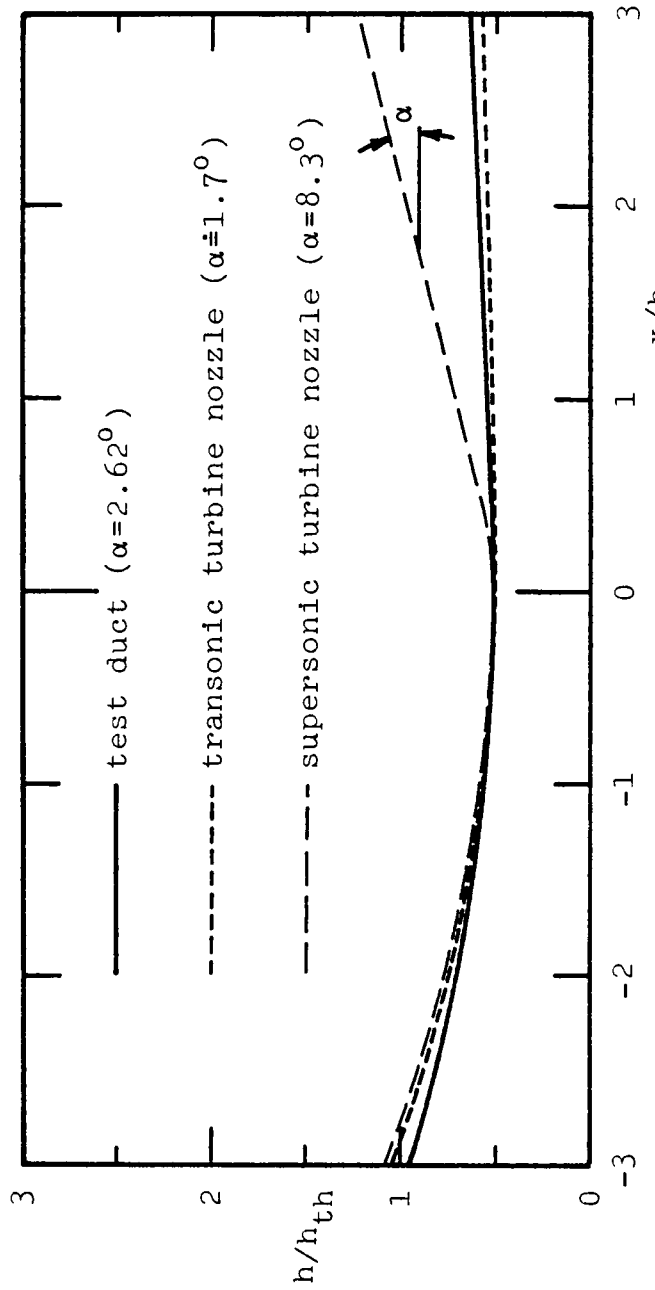


Figure 7. Comparison of Contours.

Two kinds of sidewalls are available: either with glass windows (Corning VYCOR No. 7913) for observing the shock position, or without windows but with a sequence of pressure taps to measure the wall pressures.

The entire rig is linked to UTSI (The University of Tennessee Space Institute) compressed air storage tanks by a series of pressure regulated valves, by which the air pressure is gradually reduced from approximately 3000 psig in the storage tanks to about 40 psia immediately before the combustor. The inlet pressure of the combustor can be remotely controlled within ±0.5 psi fluctuations of the desired values. The exhaust air after the test section is discharged directly into the atmosphere. The exhaust pipe is cooled by spraying water from the inner periphery to the exhausting air.

CHAPTER III

INSTRUMENTATION

The microprocessor control device located in the Transonic Wind Tunnel Laboratory at UTSI was utilized to control various aspects of the experiment.

1. Temperature Measurement

The temperatures are measured by Chromel-Alumel thermocouples (OMEGA Type K). These are located at the plenum chamber, combustor and settling chamber for total temperature measurement and, for the purpose of wall surface temperature measurement, on the top and bottom copper wall surfaces of the test section, one at the throat, one five inches upstream of the throat, and one nine inches downstream of the throat. The reference temperature, i.e., the ambient temperature, is measured by using ice point. Temperatures are scanned by a Fluke 2024-A scanner.

2. Pressure Measurement

Pressures are monitored by two alternate methods, either (a) each pressure tap is provided with its own pressure transducer (DRUCK 50 psid strain gauge type) or (b) the pressure is read through Scanivalve 48 J-91. The former method is used to monitor the total pressures of the plenum chamber, settling chamber and fuel nozzle inlet. The latter is used to measure the static pressures on the

contoured top and/or bottom walls and may be used to measure the static pressures on the sidewall.

The static pressure taps on the contoured wall are shown in Figure 8. The pressure holes, with a diameter of 1/64 inch, were spaced 0.2 inch apart in the streamwise direction and staggered 0.5 inch apart in the spanwise direction in order to reduce the mutual interference. In the downstream portion of the test section the spacings in the streamwise direction are increased to 0.4 inch apart. The number of pressure taps were 60 on top and 60 on the bottom, respectively. The pressure tap located at the last station, 8.4 inches measured from the throat, was taken as a reference point for exhaust pressure p_{ex} .

As far as the sidewall, the pressure taps are installed on it when the glass window is replaced with the windowless cover; there the pressure taps are spaced 0.25 inch apart in streamwise direction.

3. Schlieren System

A standard two-mirror Schlieren system was used to locate the shock position. The two concave mirrors have a focus of eight feet and a diameter of one foot. The spark light source has a duration of 1.5-2.5 μ seconds. The knife edge direction is normal to the main flow direction. The images are exposed to 70mm negative film (ASA 400) every 5 seconds.

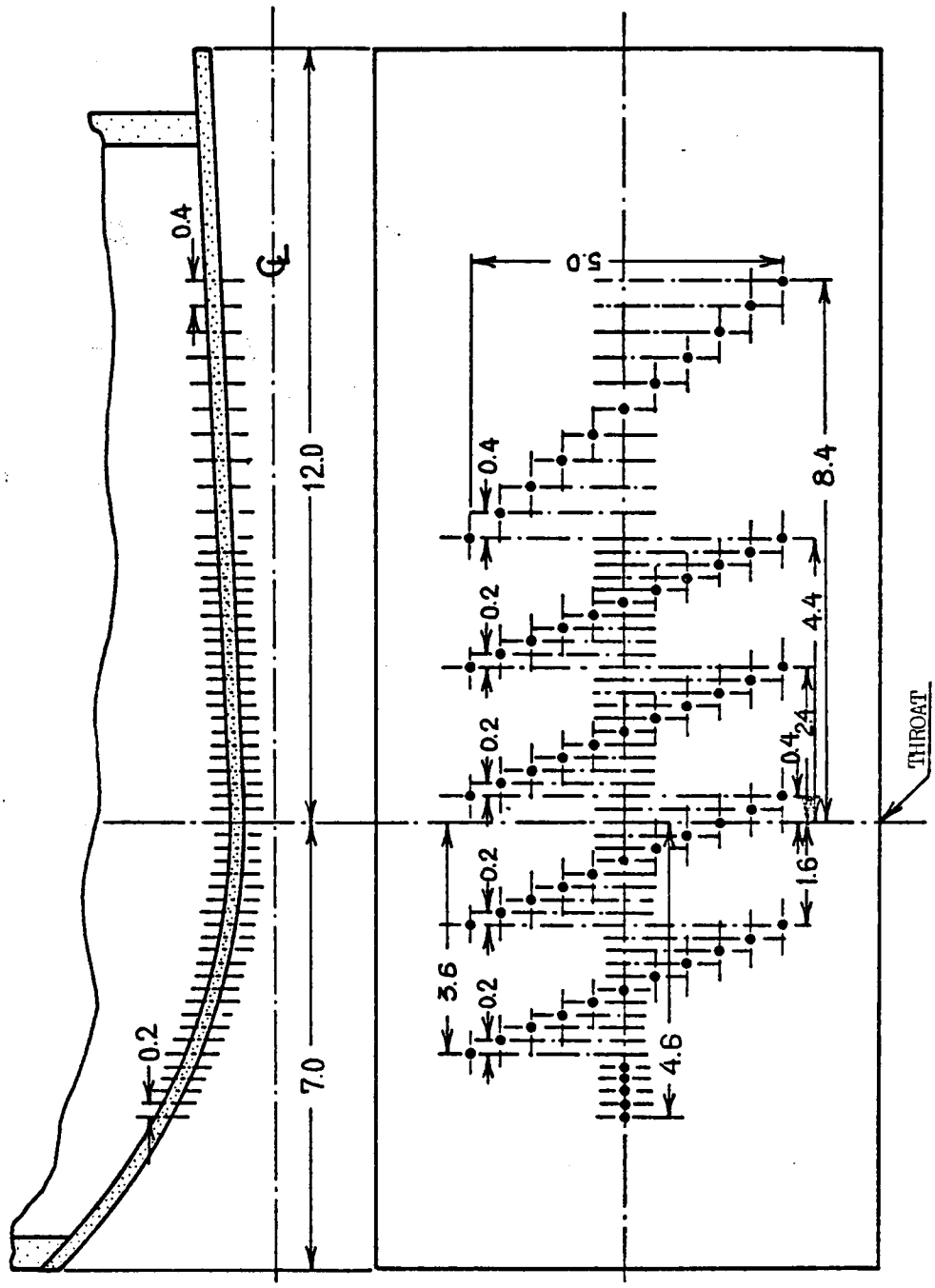


Figure 8. Pressure Taps on Top and Bottom Walls.

4. Boundary Layer Pressure Probe

The total pressure probe shown in Figure 9 was used to obtain the velocity profiles of the boundary layer. The probe is a wedge type, with six pressure holes whose diameters are 1/64 inch, with all holes located near the vertex of the wedge. The probe and support are cooled by water to prevent melting.

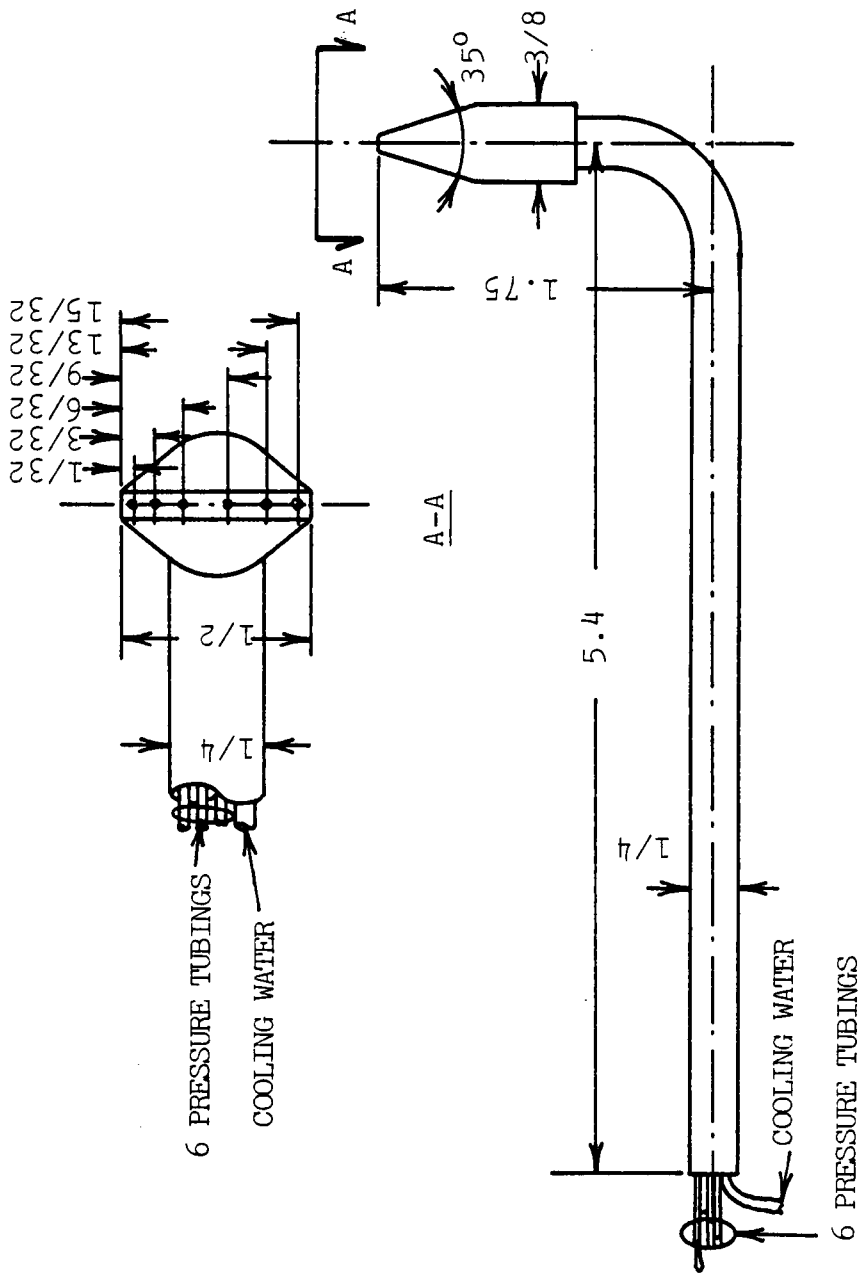


Figure 9. Total Pressure Probe.

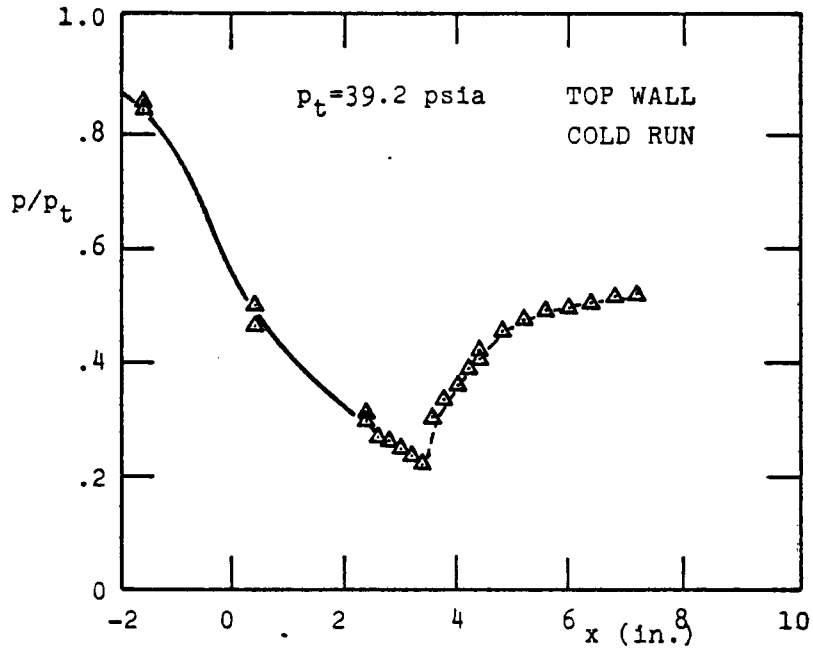
CHAPTER IV

EXPERIMENTAL RESULTS

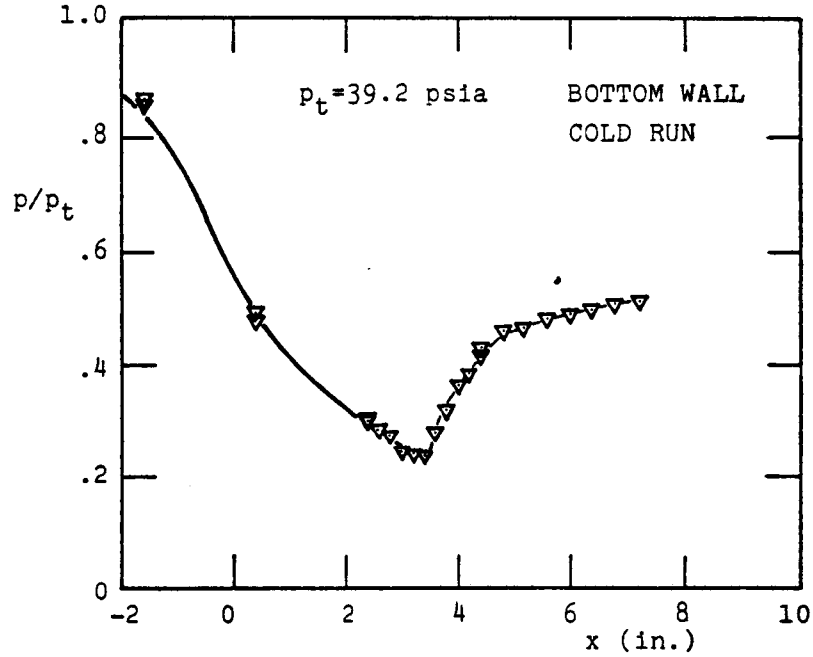
There are two important points to guard against when the tunnel is started: one is the overheating of air and the other is the generation of soot. The overheating of air can damage screens in the settling chamber. This tends to happen when the tunnel is started; at such a condition the combustion of kerosene to air mixture takes place at low air flow rate. The generation of soots in the air will not only distort Schlieren pictures but also tend to adversely insulate the contoured wall surface. Such undesirable soot production can occur in the following chain of events. Once the tunnel fails to start, unburned kerosene will flow into the diffuser, where the refractory materials will absorb it. In the next test, a large amount of soot will therefore be generated by the burning of kerosene in the refractory materials.

Once the tunnel is started, the total pressure and temperature in the settling chamber are controlled to desired values. Then the pressures and temperatures at each point are measured; at the same time either the Schlieren pictures are taken or the total pressures are measured with the boundary-layer pressure probe.

Figure 10 shows the top and bottom wall pressure distributions for a cold run. In the spanwise direction,



(a) Pressure Distribution on Top Wall



(b) Pressure Distribution on Bottom Wall

Figure 10. Pressure Distribution to Confirm Two-Dimensionality (Cold Run).

the pressure taps are distributed within a distance of five inches. The pressures at the same position x/h_{th} ($x = 0$ at throat) can be observed to be almost the same, i.e., the flow in the convergent-divergent duct has good two-dimensionality. This situation was unchanged in hot-run, and also at different back pressure control flap positions. Since the exhaust air after the test section is directly discharged to atmosphere, the expansion ratio p_e/p_t is controlled by varying total pressure p_t just upstream of the test section, i.e., at the settling chamber; it is well known that the normal shock is dependent upon the expansion ratio and at higher expansion ratio it moves upstream within the divergent section.

The pressure ratio distribution upstream of shock remains approximately the same, regardless of hot- or cold-run and cooled or heated wall. Figure 11 shows this point by way of the mean wall pressure ratio distribution upstream of shock. The data include both hot and cold runs with heat transfer; by "hot run" it is meant that the combustion is taking place in the main flow during the experiment, whereas in the "cold run" the combustion is off.

1. Experiments for Hot Run

Figures 12-15 display the observed change in the shock position by the effect of wall cooling. Two vertical

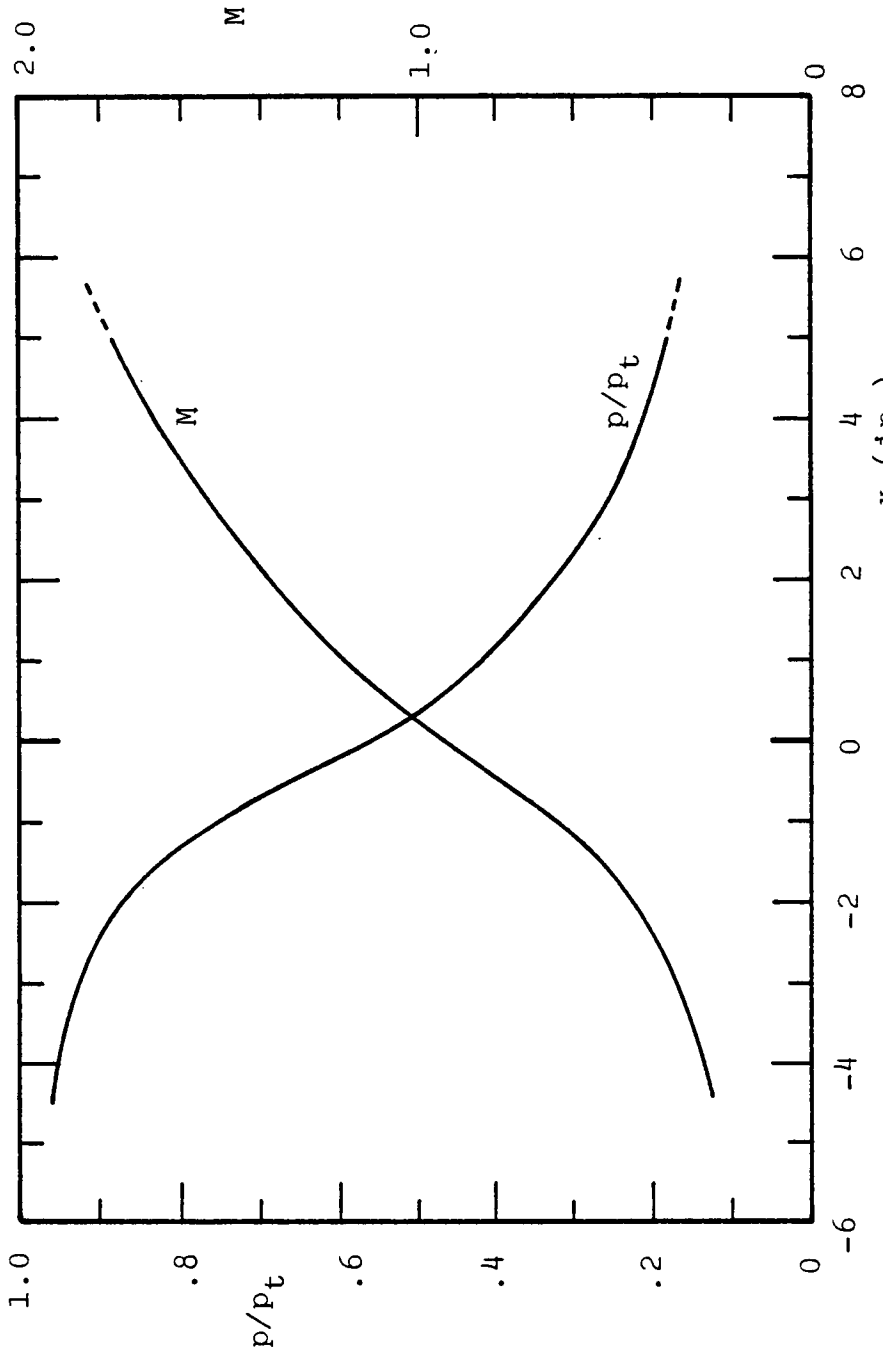
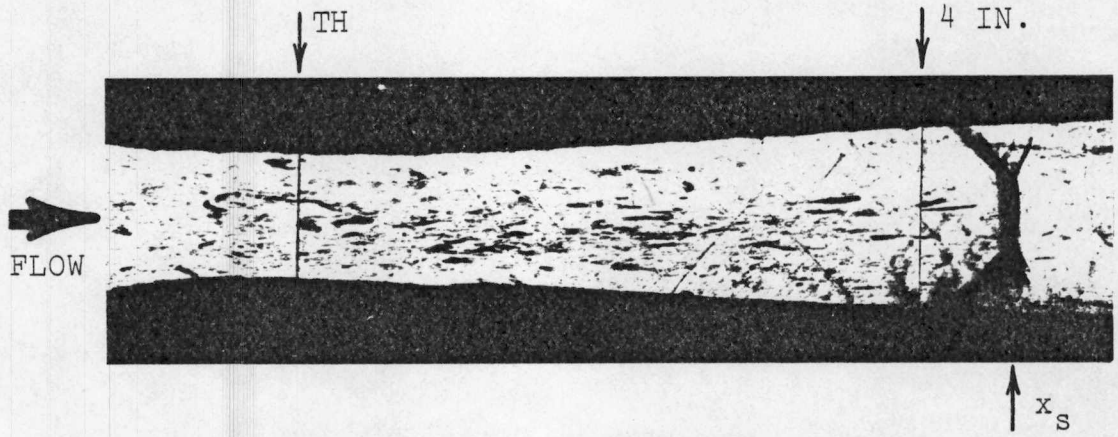
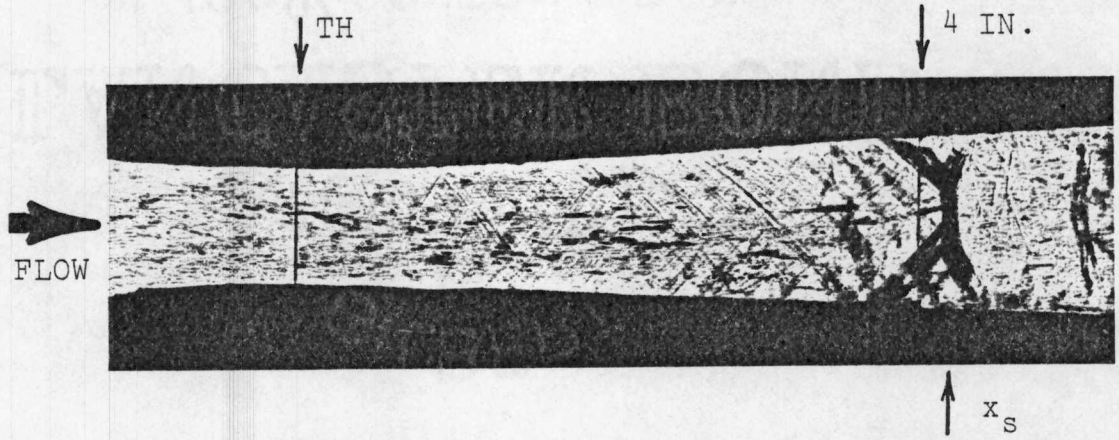


Figure 11. Mean Pressure Distribution in Test Duct.



(a) p_e/p_t=0.520 T_w/T_t=0.481 x_s/h_{th}=5.10
with cooling



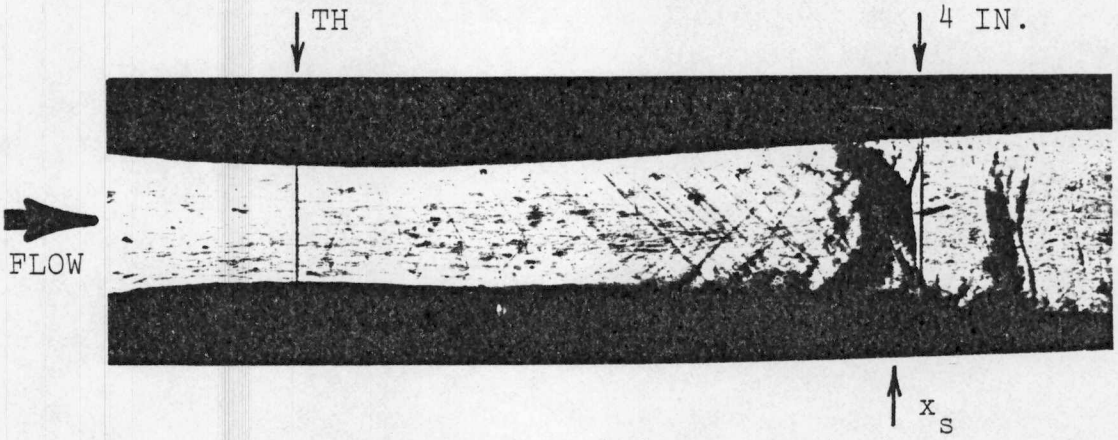
(b) p_e/p_t=0.525 T_w/T_t=0.625 x_s/h_{th}=4.67
without cooling

TH: Markers at Throat

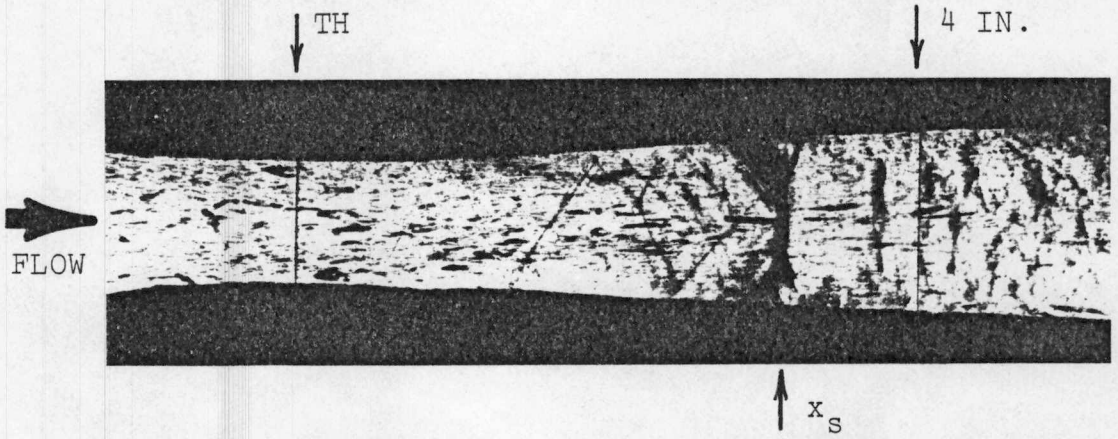
4 IN.: Markers at 4 in. Downstream of Throat

x_s: Shock Positions

Figure 12. Shock Location (Hot Run);
p_e/p_t = 0.520, p_e/p_t = 0.525.



(a) p_e/p_t=0.597 T_w/T_t=0.498 x_s/h_{th}=4.24
with cooling



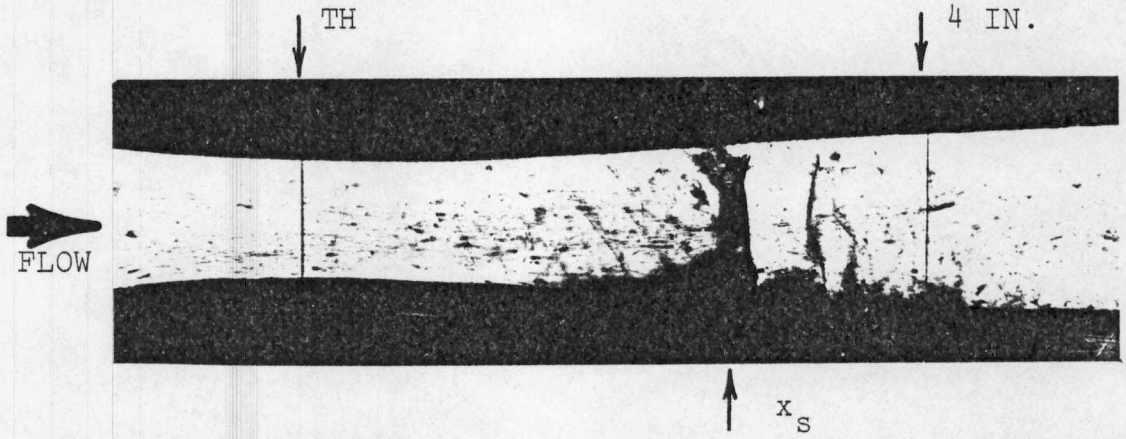
(b) p_e/p_t=0.595 T_w/T_t=0.652 x_s/h_{th}=3.47
without cooling

TH: Markers at Throat

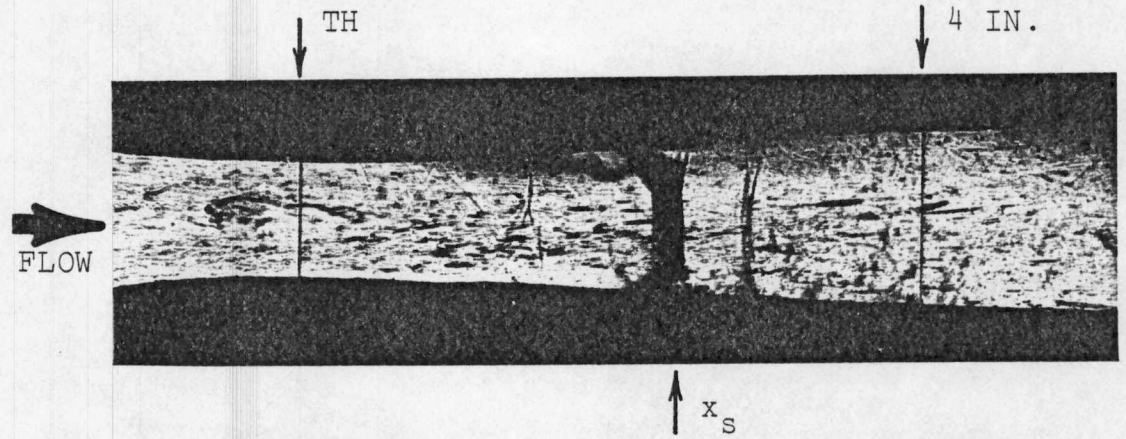
4 IN.: Markers at 4 in. Downstream of Throat

x_s: Shock Positions

Figure 13. Shock Location (Hot Run);
p_e/p_t = 0.597, p_e/p_t = 0.595.



(a) p_e/p_t=0.663 T_w/T_t=0.461 x_s/h_{th}=3.07
with cooling



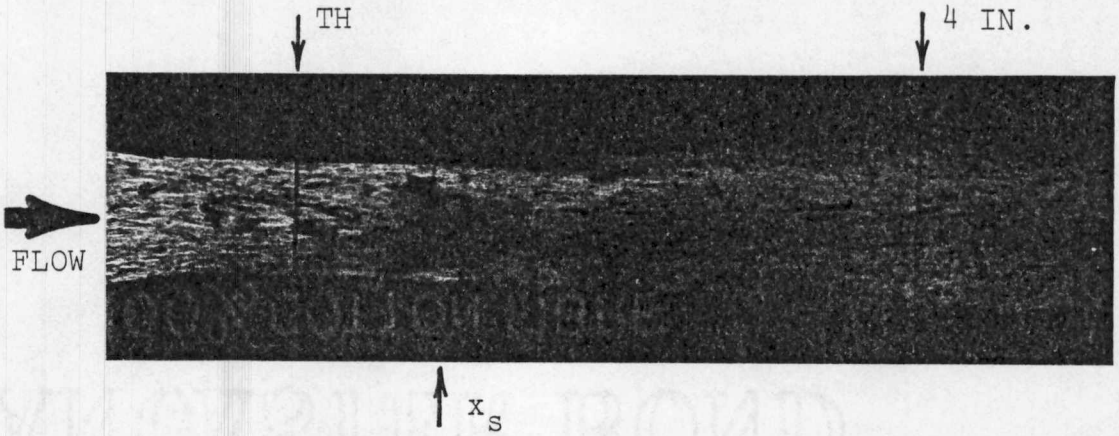
(b) p_e/p_t=0.669 T_w/T_t=0.685 x_s/h_{th}=2.62
without cooling

TH: Markers at Throat

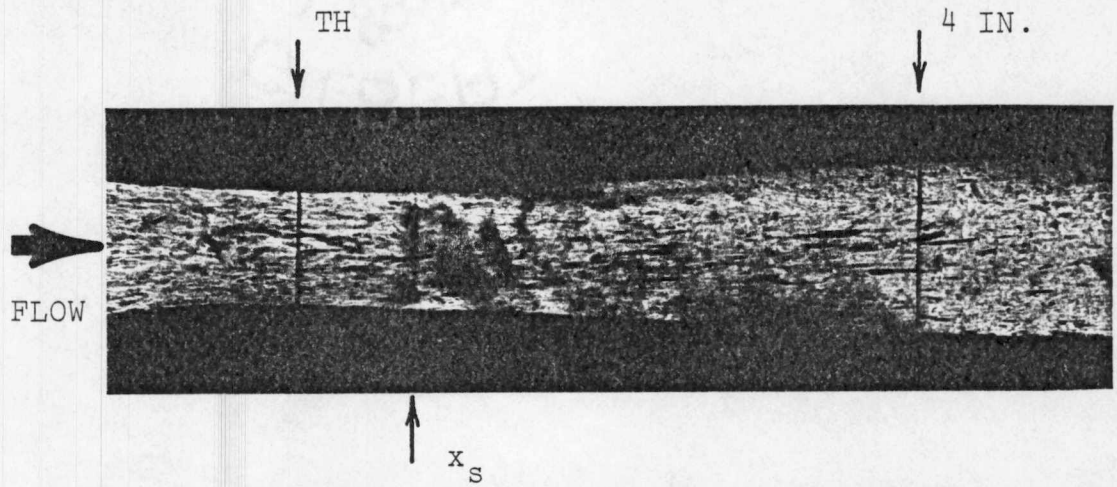
4 IN.: Markers at 4 in. Downstream of Throat

x_s: Shock Positions

Figure 14. Shock Location (Hot Run);
p_e/p_t = 0.663, p_e/p_t = 0.669.



(a) p_e/p_t=0.800 T_w/T_t=0.461 x_s/h_{th}=0.98
with cooling



(a) p_e/p_t=0.800 T_w/T_t=0.672 x_s/h_{th}=0.95
without cooling

TH: Markers at Throat

4 IN.: Markers at 4 in. Downstream of Throat

x_s: Shock Positions

Figure 15. Shock Location (Hot Run);
p_e/p_t = 0.800.

lines are markers--one is at the throat and the other four inches downstream of it; the flow direction is from left to right. The flow conditions corresponding to these figures are given in Table 3.

Figure 12 corresponds to the low pressure ratio of $p_e/p_t = 0.52$. The presence of normal shock is observed in the mainstream. Near the wall an oblique shock is formed slightly upstream of the normal shock. Further downstream, just behind the normal shock, the second bifurcated leg of the normal shock is formed. By making comparison of Figure 12(a) for a cooled wall with (b) for an uncooled wall, one observes that the effect of wall-cooling shifts the position of normal shock in the downstream direction.

As p_e/p_t is increased the shock moves upstream, as seen from the sequence of Figure 13 through Figure 15. In Figure 15 no oblique shock is observed. However, one still observes that the effect of cooling slightly shifts the position of the normal shock.

Figure 16 summarizes these observed shifts in the shock position, including the results for other flow conditions and various positions of the back pressure control flap. The degree of wall cooling is categorized in the following five ranges: $T_w/T_t = 0.3\text{-}0.4$, $0.4\text{-}0.5$, $0.5\text{-}0.6$, $0.6\text{-}0.7$ and $0.7\text{-}0.8$. The two straight lines represent the least square curve fit of data falling in the ranges of $T_w/T_t = 0.4\text{-}0.5$ and $0.7\text{-}0.8$. It is observed

TABLE 3

FLOW CONDITIONS CORRESPONDING TO FIGURES 12-15 (HOT RUN)

Figure	Condition	p_t psia	p_e psia	p_e/p_t	T_t °R	T_w °R	T_w/T_t	x_s/h_{th}
12 (a)	with cooling	28.8	15.0	0.520	1396.1	671.5	0.481	5.10
12 (b)	without cooling	28.8	15.1	0.525	1114.2	746.0	0.652	4.67
13 (a)	with cooling	25.8	15.4	0.597	1207.8	601.5	0.498	4.24
13 (b)	without cooling	25.5	15.2	0.595	1155.0	753.1	0.652	3.47
14 (a)	with cooling	22.8	15.1	0.663	1191.7	549.4	0.461	3.07
14 (b)	without cooling	22.4	15.0	0.669	1396.8	956.8	0.685	2.62
15 (a)	with cooling	19.0	15.2	0.800	1484.0	684.1	0.461	0.98
15 (b)	without cooling	18.4	14.7	0.800	1392.7	935.9	0.672	0.95

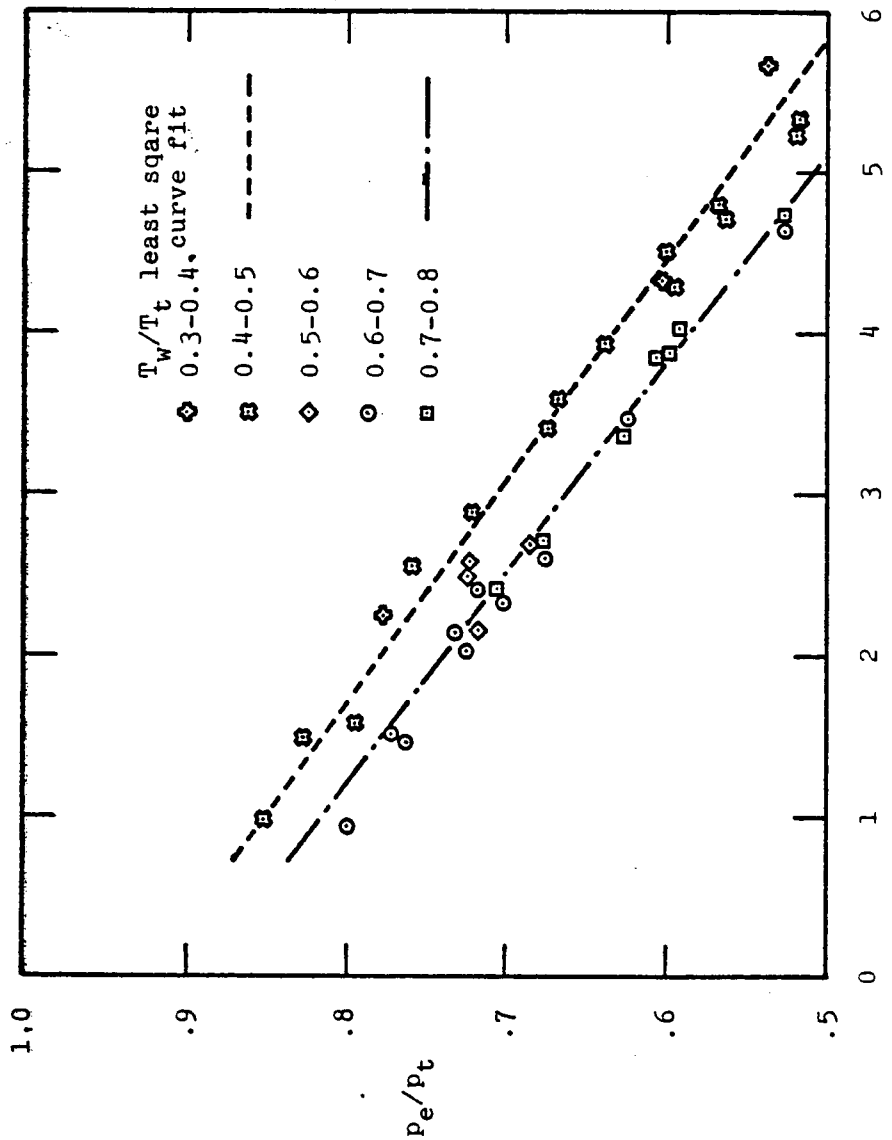


Figure 16. Relationship of Shock Location with Expansion Ratio and Temperature Ratio (Hot Run).

that the colder the wall, the more the amount of downstream shift in the shock position. Because of the use of the copper wall surrounding the test section, it is difficult to achieve the truly adiabatic wall condition; therefore, the highest temperature ratio attainable is below 0.9.

Corresponding to the shock patterns of Figures 12-15, Figures 17-20 show the static wall pressure distribution along the top wall of the duct. Throughout these, the pressure distributions upstream of shock remain almost the same, as mentioned before. From these results, the sonic line position is virtually unaffected by the effect of the cooling wall. The boundary layer is negligibly thin and the heat transfer rate is small; as detailed in the subsequent discussion in Chapter V, these tend to minimize the shift in sonic line. Upstream of shock including the throat region, the pressure distribution remains unaffected by cooling. However, downstream of the shock the pressure rise is affected by the cooling; for the cold wall the pressure downstream of the shock is, for the most part, lower than that of the uncooled wall except near the exhaust, where the two pressure distributions become identical.

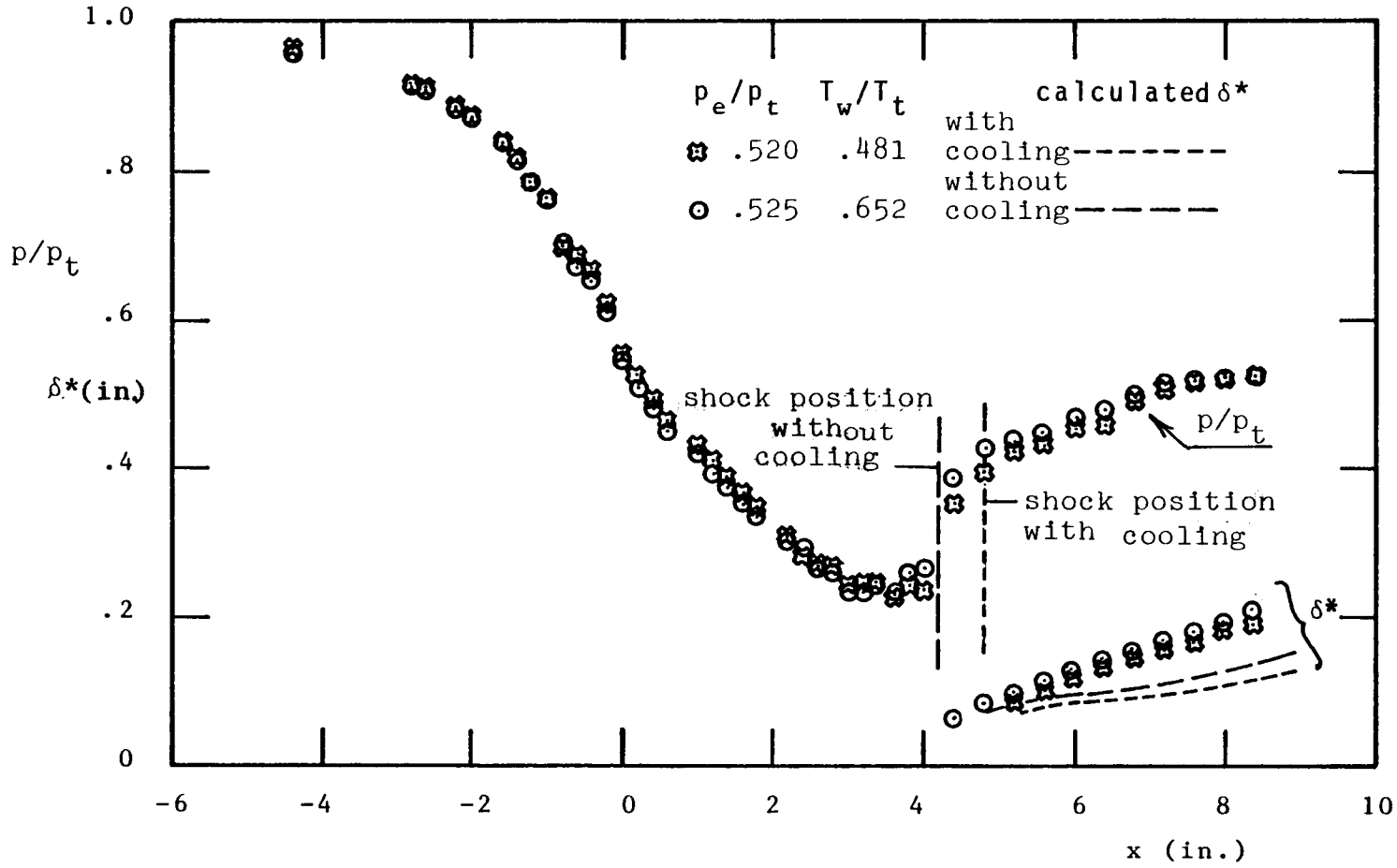


Figure 17. Pressure Distribution and Displacement Thickness (Hot Run); $p_e/p_t = .520$, $p_e/p_t = .525$.

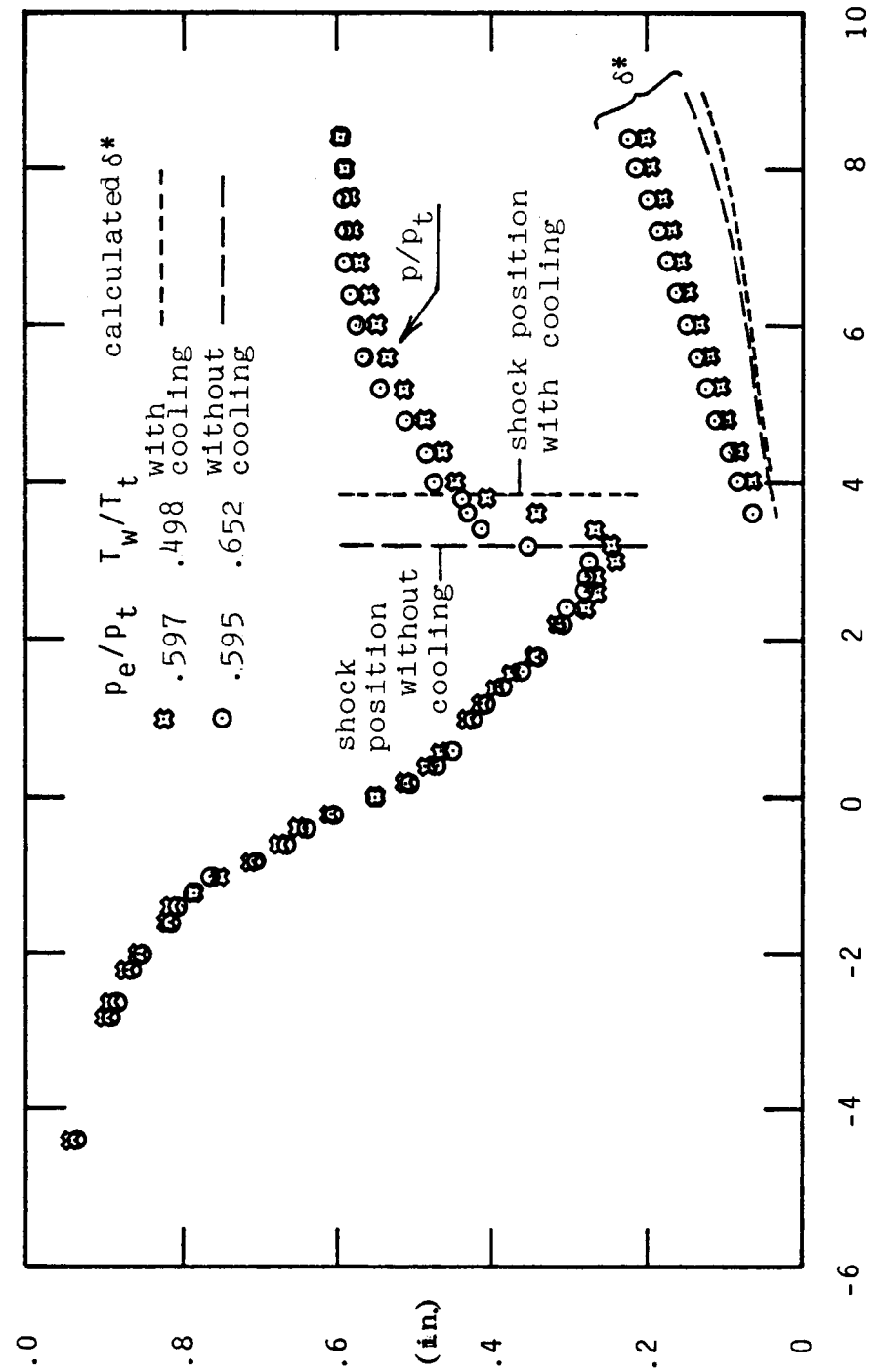


Figure 18. Pressure Distribution and Displacement Thickness (Hot Run); $p_e/p_t = .597$, $p_e/p_t = .595$.

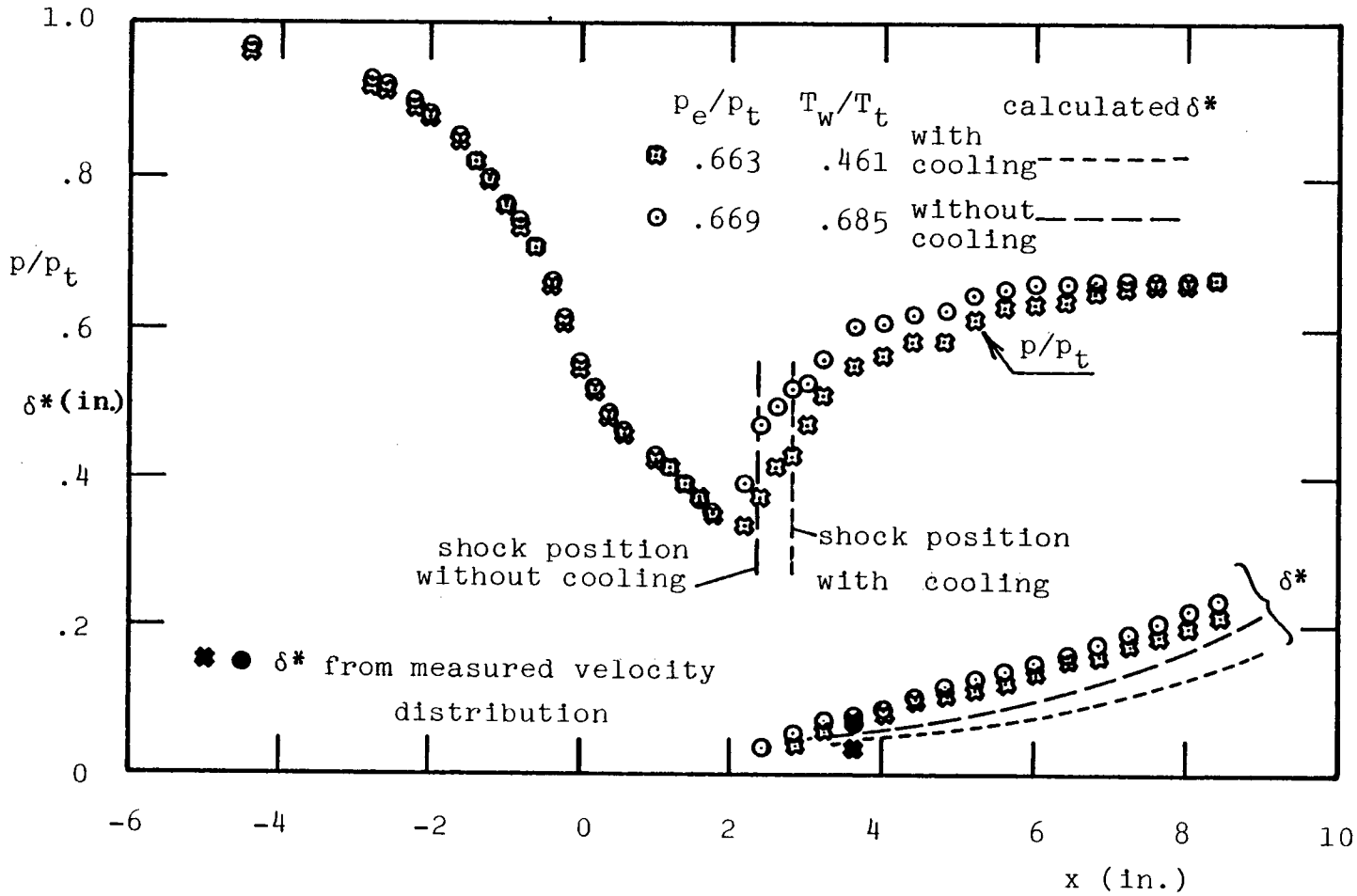


Figure 19. Pressure Distribution and Displacement Thickness (Hot Run); $p_e/p_t = .663$, $p_e/p_t = .669$.

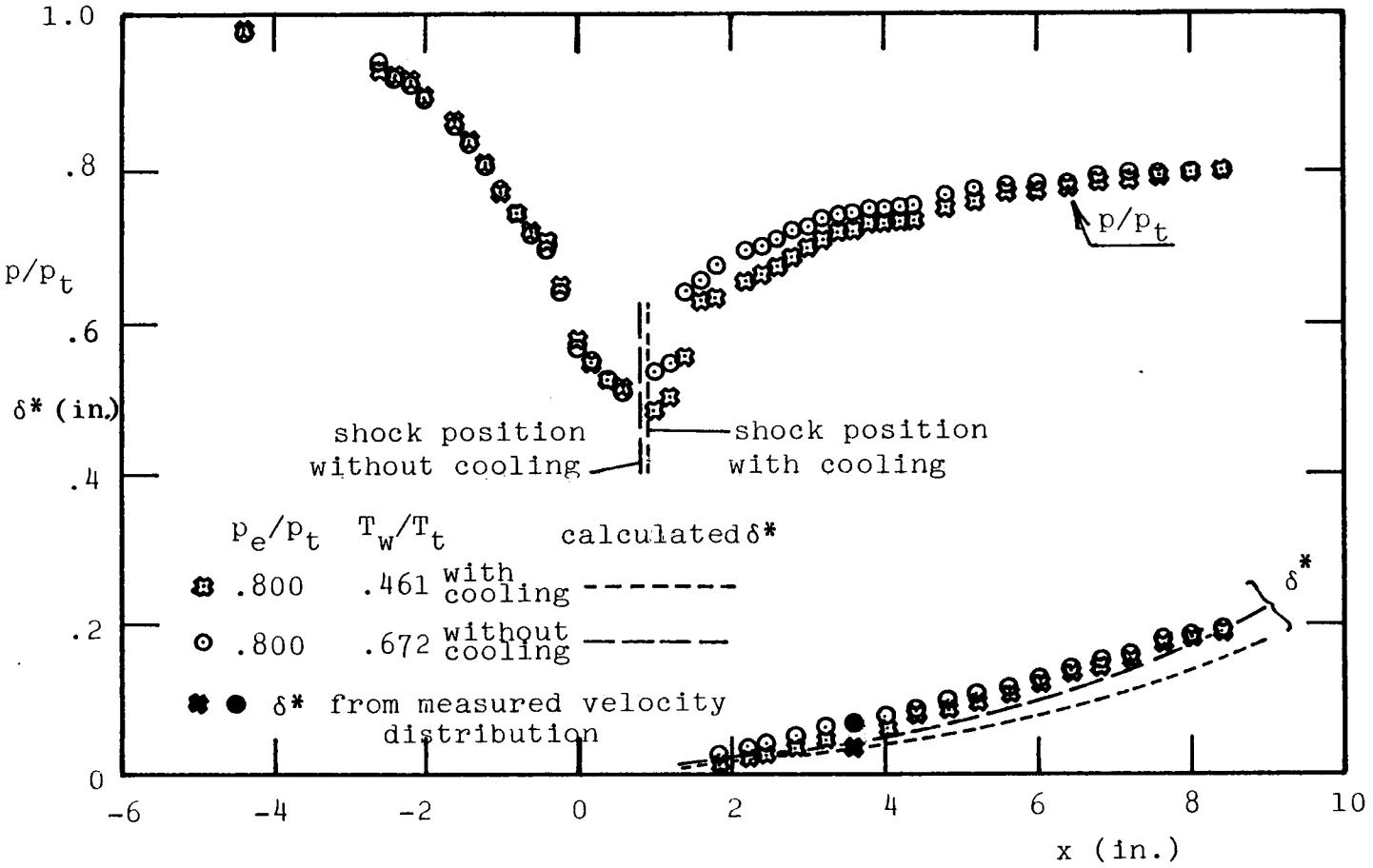
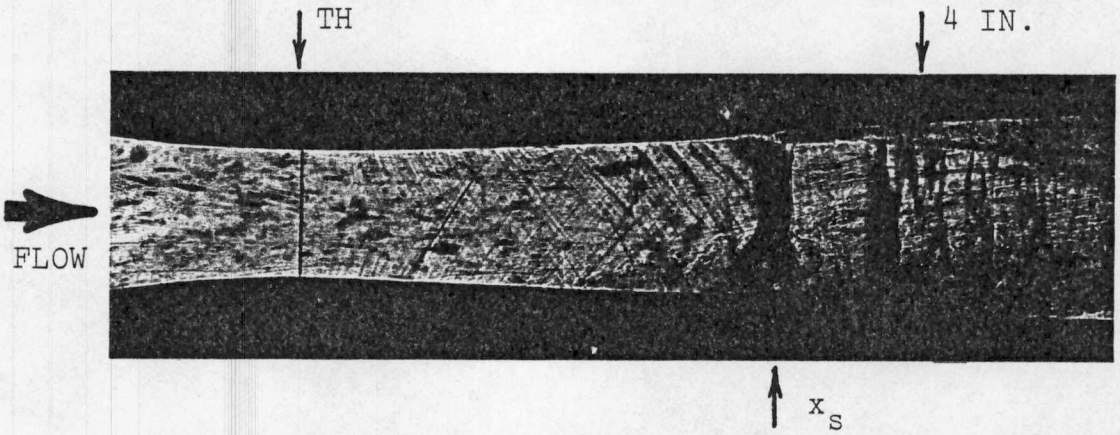


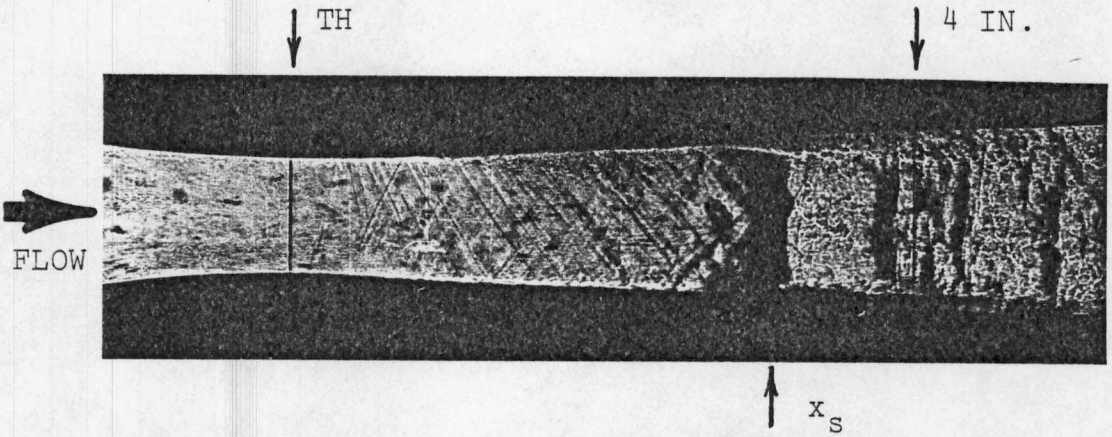
Figure 20. Pressure Distribution and Displacement Thickness (Hot Run).

2. Experiments for Cold Run

For cold run, where the combustion does not take place in the main flow, the wall temperatures are maintained almost the same as main flow total temperature by emptying the coolant water from the jacket; in certain runs the wall temperature is raised by electric heaters surrounding the test section. Figure 21 shows the effects of wall temperature; the detailed flow conditions are given in Table 4. One observes that, as before, the normal shock has the bifurcated oblique shocks near the wall but, in addition, a number of weak normal shocks appear further downstream of bifurcated normal shock. In comparison to hot run corresponding to the same shock position (see Figure 13, page 28), these weak shocks become more distinct in cold run than those of hot run. The change in the shock position by the effect of wall heating is insignificant. The wall pressure distributions are almost the same as shown in Figure 22. Figure 23 shows the summarized results of the shock position, including those of other flow conditions. Since the effects of heating wall were not the main objective, this was examined only over limited range of wall-to-main flow temperature ratio. In the range of temperature ratio no significant change in the shock position by the effect of wall heating was observed. However, it turns out that the cold flow shifts the shock position to downstream direction as compared to



(a) p_e/p_t=0.648 T_w/T_t=0.991 x_s/h_{th}=3.39
without heating



(b) p_e/p_t=0.653 T_w/T_t=1.288 x_s/h_{th}=3.41
with heating

TH: Markers at Throat
4 IN.: Markers at 4 in. Downstream of Throat
x_s: Shock Positions

Figure 21. Shock Location (Hot Run);
p_e/p_t = 0.648, p_e/p_t = 0.653.

TABLE 4

FLOW CONDITIONS CORRESPONDING TO FIGURE 21 (HOT RUN)

Figure	Condition	p_t psia	p_e psia	p_e/p_t	T_t °R	T_w °R	T_w/T_t	x_s/h_{th}
21 (a)	without heating	24.4	15.8	0.648	522.9	518.2	0.991	3.39
21 (b)	with heating	23.6	15.4	0.653	533.5	687.1	1.288	3.41

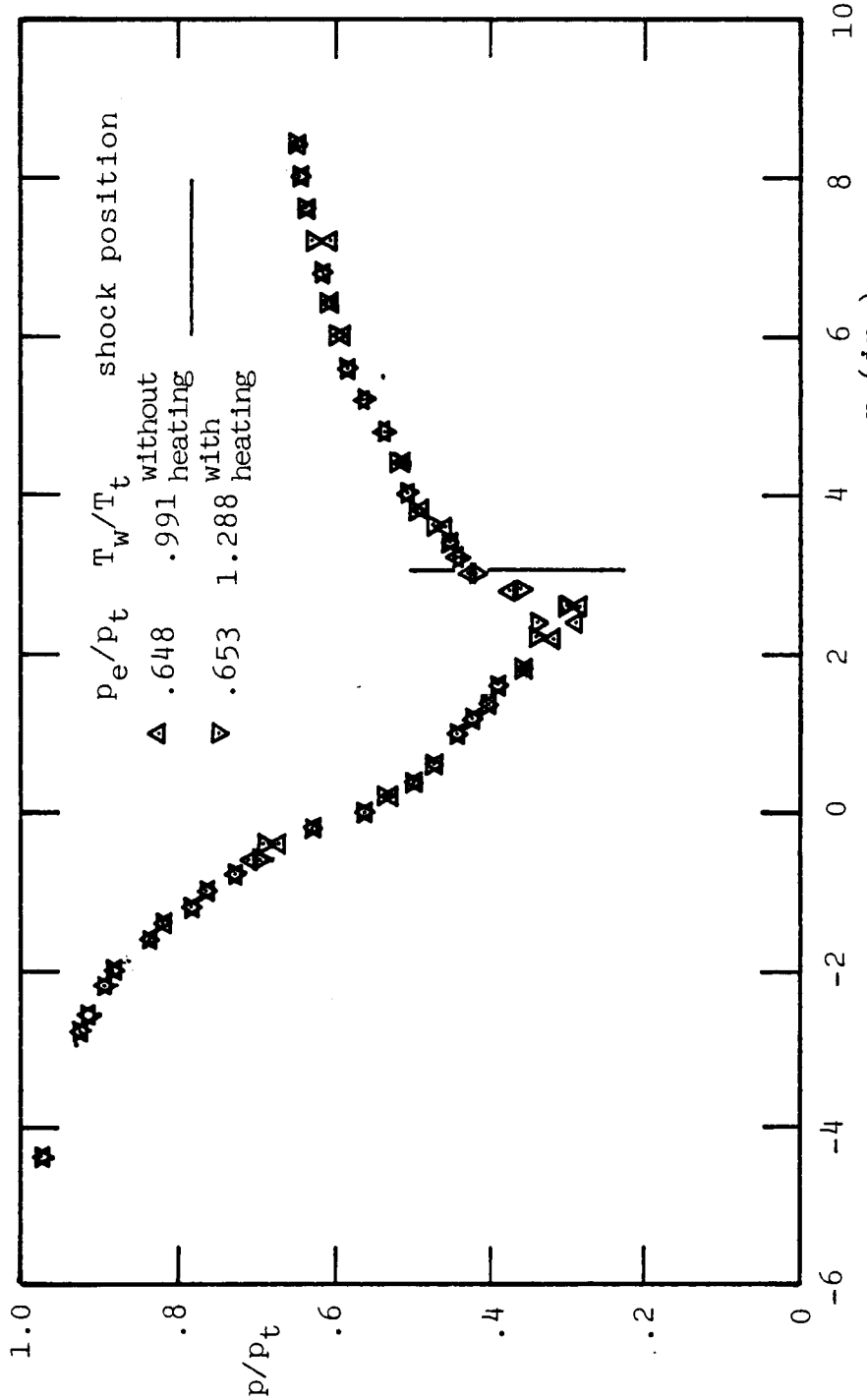


Figure 22. Pressure Distribution (Cold Run).

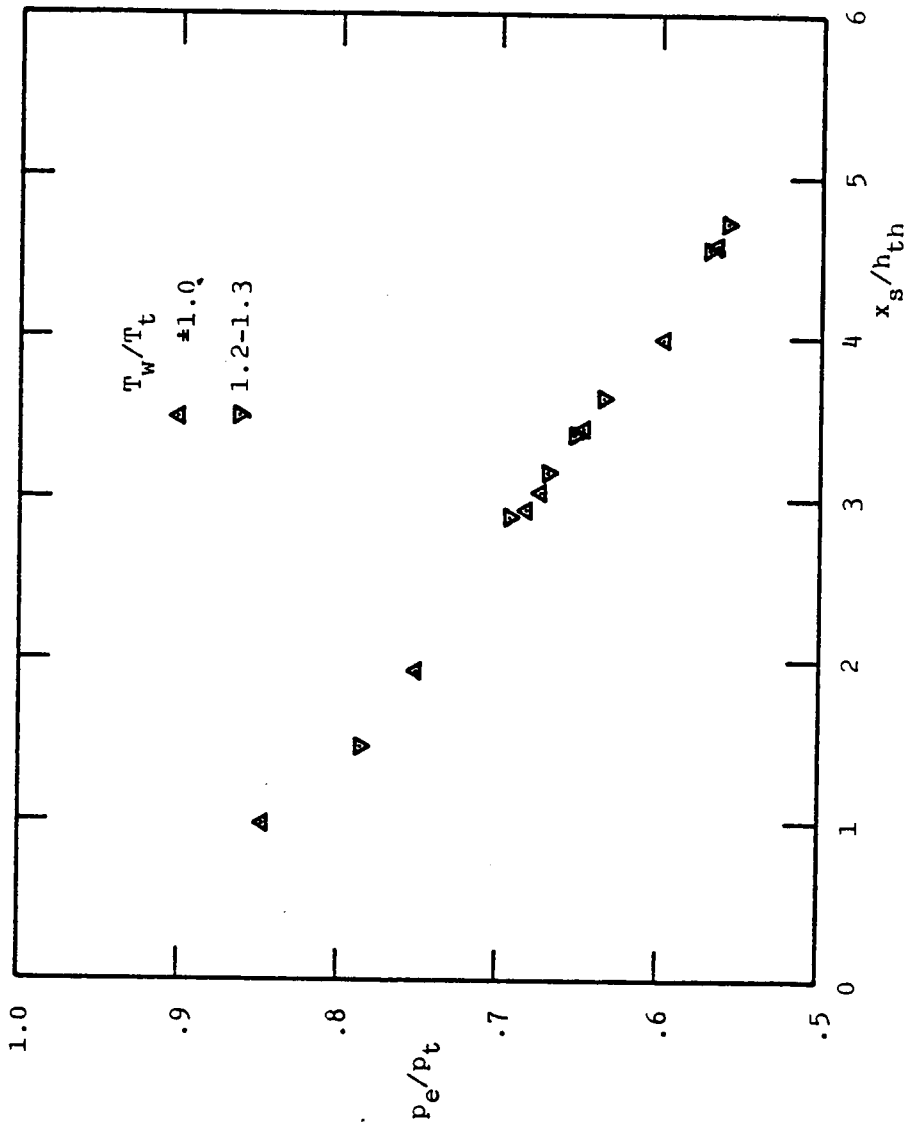


Figure 23. Relationship of Shock Position with Expansion Ratio and Temperature Ratio (Cold Run).

the hot run data in the temperature ratio range of 0.7-0.8 (Figure 16, page 33).

CHAPTER V

DISCUSSION OF EXPERIMENTAL RESULTS

1. Sonic Location

First we apply the one-dimensional approximation to the inviscid flow through a streamtube where heat transfer is taking place [11] and obtain

$$\frac{du}{u} = \frac{1}{1 - M^2} \left(\frac{dQ}{c_p T} - \frac{dA}{A} \right) \quad , \tag{5.1}$$

where du, dQ and dA are the changes of u, Q and A in the streamwise direction, respectively. In general, choking occurs when M = 1. And shift in the sonic location due to heat transfer is given by [14],

$$\frac{dA}{A} = \frac{dQ}{c_p T} \quad . \tag{5.2}$$

Applied to the present test conditions, the change of sonic location turns out to be only between x = -0.02 and x = 0.01 inch. Therefore, the sonic line still remains virtually at the throat (the approximate calculation is discussed in Appendix A). This point is seen by referring back to Figure 11, page 26, where the wall pressure at the throat remains the same for all runs, including the tests with and without heat transfer.

2. Shape of Boundary Layer Profiles

Before proceeding to the discussion of viscous and heat transfer effects, it is necessary to identify whether the flow is laminar or turbulent in order to ascertain that the cooling does not inadvertently alter such fundamental characteristics of the flow. The combustion in general makes the flow turbulent, as discussed in Chapter II. However, even if the incoming flow is turbulent, the presence of favorable pressure gradient can revert it to the laminar flow [15-18]. This is the so-called relaminarization, where a reversion from turbulent to laminar flow takes place by the presence of acceleration. A measure of acceleration or the freestream acceleration parameter K is, in general, defined as [16]

$$K = \frac{\mu_e}{\rho_e u_e^2} \frac{d u_e}{dx} \quad , \tag{5.3}$$

and, if this exceeds a critical value, relaminarization takes place. Figure 24 shows the acceleration parameter K at the throat, where it takes almost maximum value in the present test section. The critical value of K is given as 2.88×10^{-6} for a conical nozzle [16]. For a two-dimensional flow applicable to the present case, assuming that the critical value of K occurs at the critical Reynolds

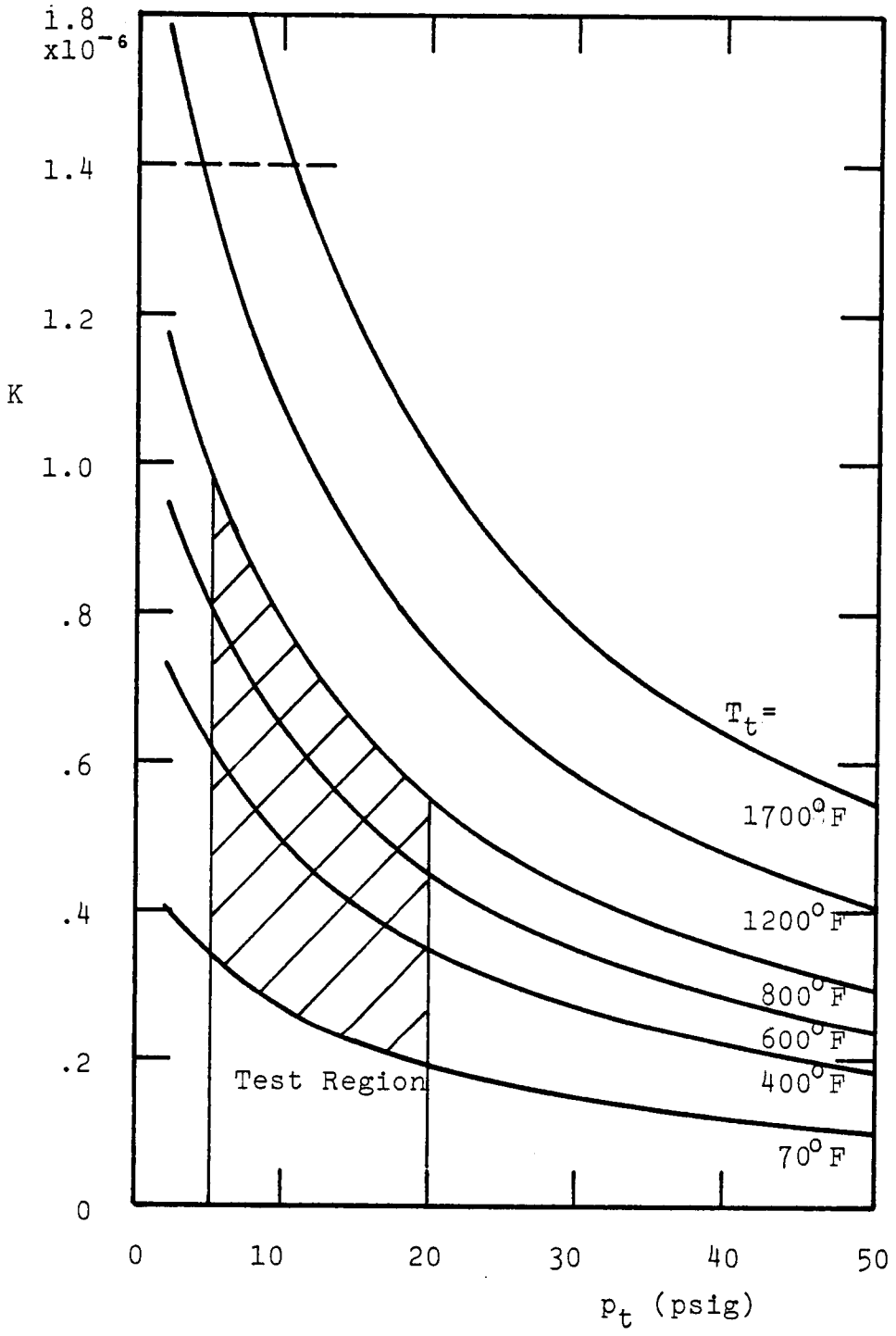


Figure 24. Acceleration Parameter at Throat.

number based on momentum thickness over the flat plate, the critical value of K decreases to 1.4×10^{-6} as shown in Appendix B. As shown in Figure 24, the value of K in the present test conditions is less than 1×10^{-6} . In any event, regardless of whether one uses two- or three-dimensional flow criteria, the value of K is less than critical and the flow appears to remain always turbulent. Another supporting evidence for this comes from the velocity profile measurements which will be discussed below.

Figure 25 shows the velocity profiles near the wall for cold run; the data at x = -1.0 inch correspond to several expansion ratios between 0.455 and 0.732. For hot run, the velocity profiles downstream of the shock are shown in Figure 26. Both are plotted in the typical "law of the wall" representation in terms of u^+, T^+ and y^+, which are defined by

$$u^+ = \frac{u_b}{u_\tau} \quad , \quad T^+ = \frac{T_w - T_b}{\frac{q_w}{\rho_w \, u_t \, c_{p,w}}} \quad , \quad y^+ = \frac{\rho_w \, u_\tau \, y}{\mu_w} \quad , \quad (5.4)$$

respectively, where u_τ is the frictional velocity given by $u_\tau^2 = \tau_w/\rho_w$. In Figure 25, the velocity outside of boundary layer at x = -1.0 inch is always subsonic ($M \simeq 0.7$). However, at x = 2.3 inches,

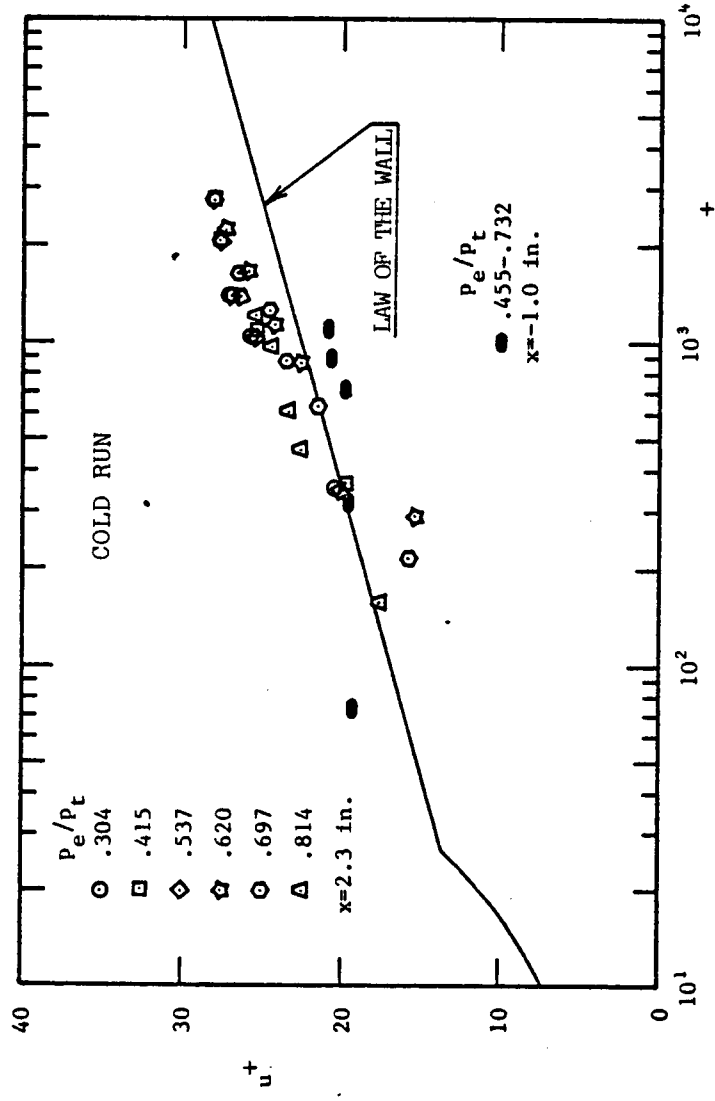


Figure 25. Velocity Distribution at x = -1.0 and 2.3 Inches (Cold Run).

the velocity outside of boundary layer may change flow from supersonic ($M \simeq 1.4$) for low expansion ratio; the latter is due to the fact that the traverse location lies downstream of the normal shock. It is clear from these observations that the velocity distributions near the throat follow the "law of the wall."

In Figure 26, the velocity distributions again conform to the "law of the wall"; the temperature distribution is, however, slightly lower than the "law of the wall." The reason for this small discrepancy is unclear; the temperature is calculated based on measured velocity profiles. In any case, the agreement of the data with the "law of the wall" indicates again that the flow remains turbulent. In addition to Figures 25 and 26, the following evidences serve to confirm the fact that the flow is always turbulent: (a) the lack of any noticeable change due to the boundary layer trip (1/32-inch diameter) installed either inlet of the test section or at 2 inches upstream of the throat; (b) the presence of vigorous disturbance due to combustion process; and (c) the agreement of the data for the oblique shock angle discussed in the next section.

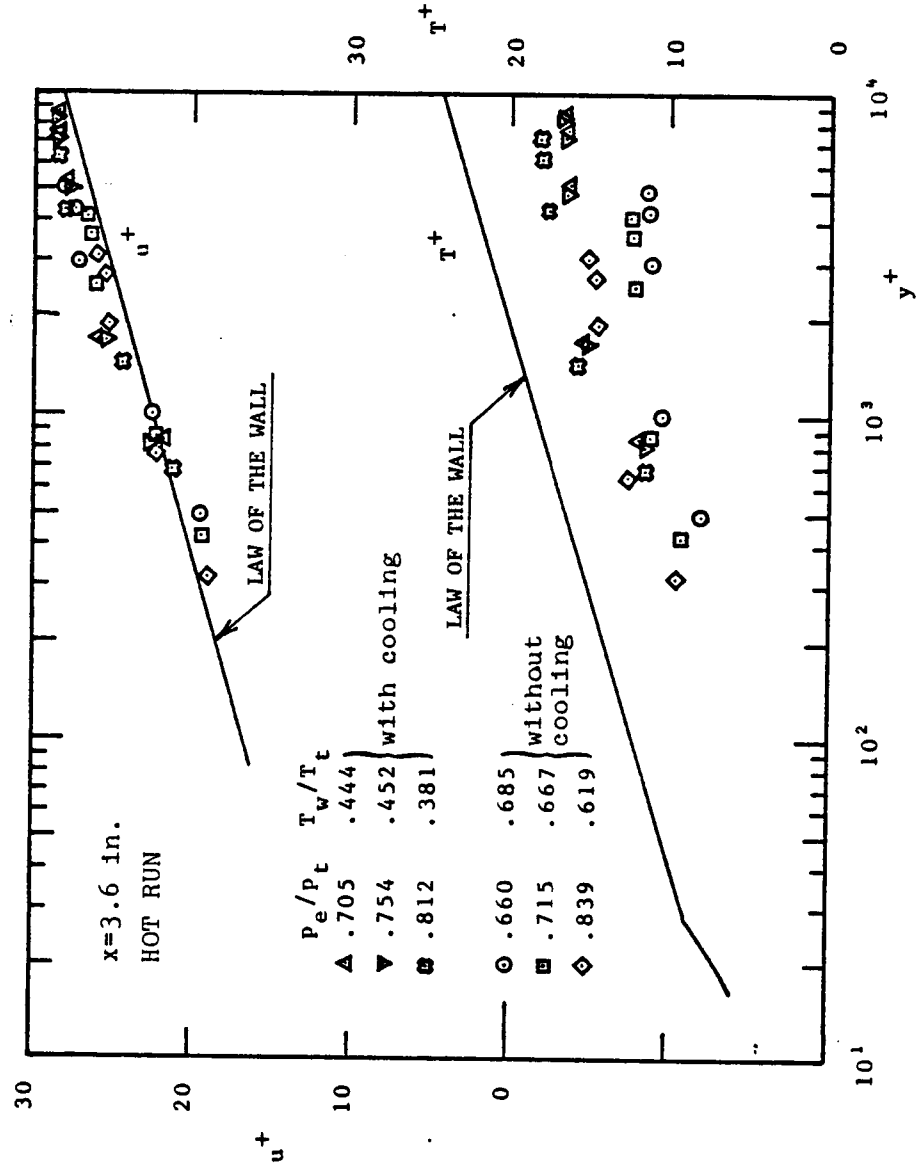


Figure 26. Velocity and Temperature Distribution Downstream of Shock (x = 3.6 Inches) (Hot Run).

3. Schlieren Observation

The freestream pressure rise through the shock produces a separation which, in turn, increases the boundary layer thickness. This increase of boundary layer thickness induces weak oblique shock [19-21] near the wall region of a normal shock. Figure 27 shows the oblique shock measured from Schlieren pictures. Solid lines are calculated by Mager's equation [19],

$$\frac{p_s}{p_1} = 1 + \frac{\gamma M_1^2}{2} \frac{0.506}{1 + \frac{\gamma-1}{2} M_1^2} \qquad \text{for } M_1 \gtrsim \sqrt{2} \quad . \qquad (5.5)$$

A favorable agreement is seen between the observed oblique shock angle (ϕ) and the one based on Mager's turbulent separation criterion (although, strictly speaking, it has to be borne in mind that the Mager's criterion is derived without taking the effect of heat transfer into consideration).

4. Boundary Layer Thickness

Boundary layer velocity and temperature distributions are already shown in Figures 25 and 26 and the flow was found to be always turbulent, as described in Section 2 of this Chapter. We will now discuss the displacement thickness for the cold

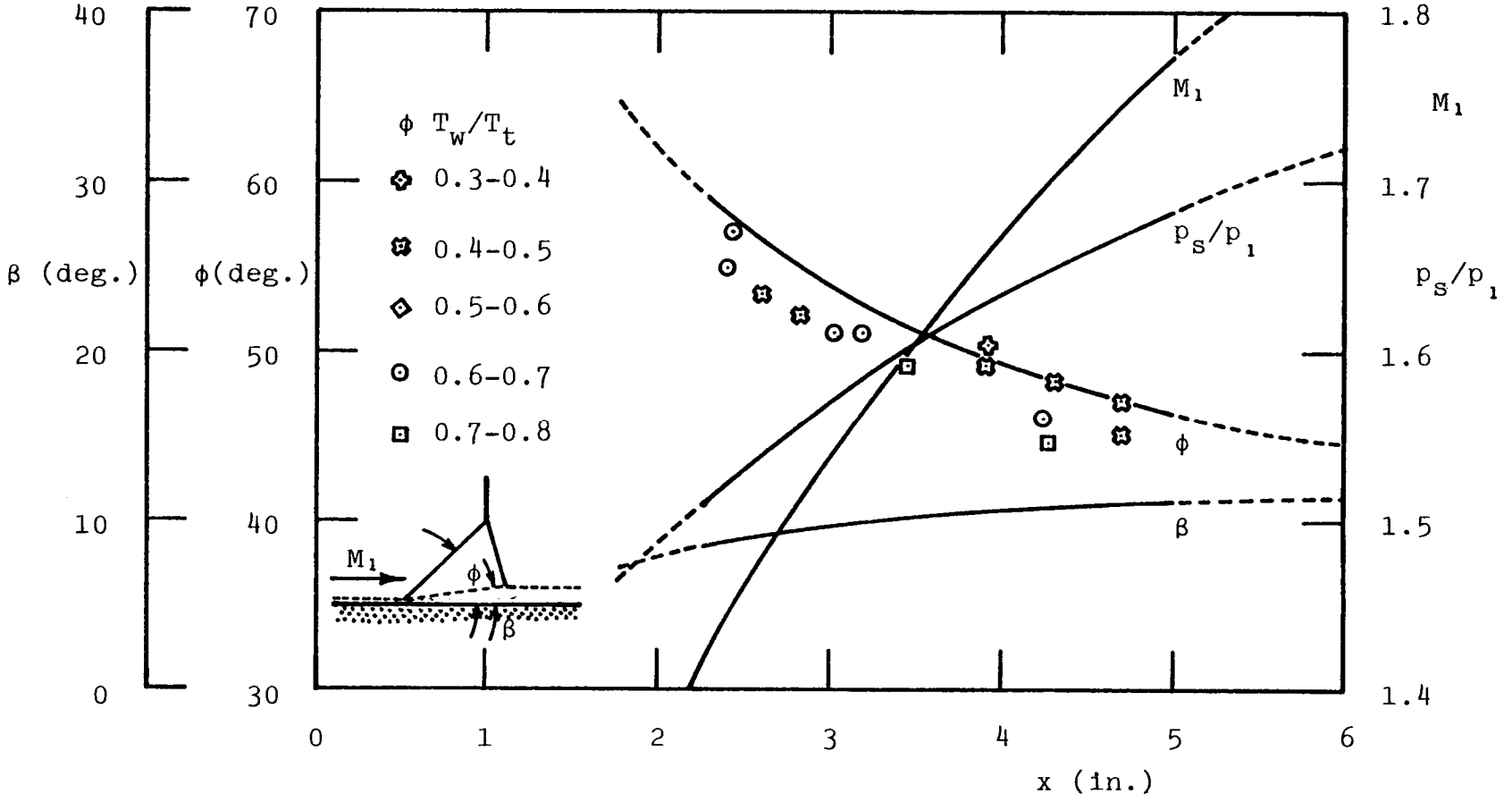


Figure 27. Bifurcated Oblique Shock Angle.

and hot run, further details of which are in Appendices D and F.

Cold Run. From boundary layer measurement at $x = 2.3$ inches, corresponding to the upstream position of the shock for the cold run indicated in Figure 25, the value of the displacement thickness δ^* there calculated by equation (D.3) in Appendix D is about 0.014 inches (this corresponds to the values of $p_e/p_t = 0.304$, 0.415 and 0.537). For $p_e/p_t = 0.814$, the position corresponding to $x = 2.3$ inches is now located downstream of the shock; there, displacement thickness δ^* becomes 0.032 inches. The ratio of displacement thickness between downstream and upstream of the normal shock is about $0.032/0.014 = 2.3$.

Hot Run. For hot run, the displacement thickness measurements at $x = 3.6$ inches for different expansion ratio p_e/p_t and temperature ratio T_w/T_t are shown in Figure 28. The normal shock is always located upstream of measuring position ($x = 3.6$ inches). The values of displacement thickness there are 0.061 inches without cooling and 0.031 inches with cooling wall. These values are almost the same regardless of different shock locations or expansion ratio. Notice that the difference of the displacement thickness between the one with cooling and without cooling is sizeable. The displacement thickness δ^* with cooling wall is thinner than that without cooling wall.

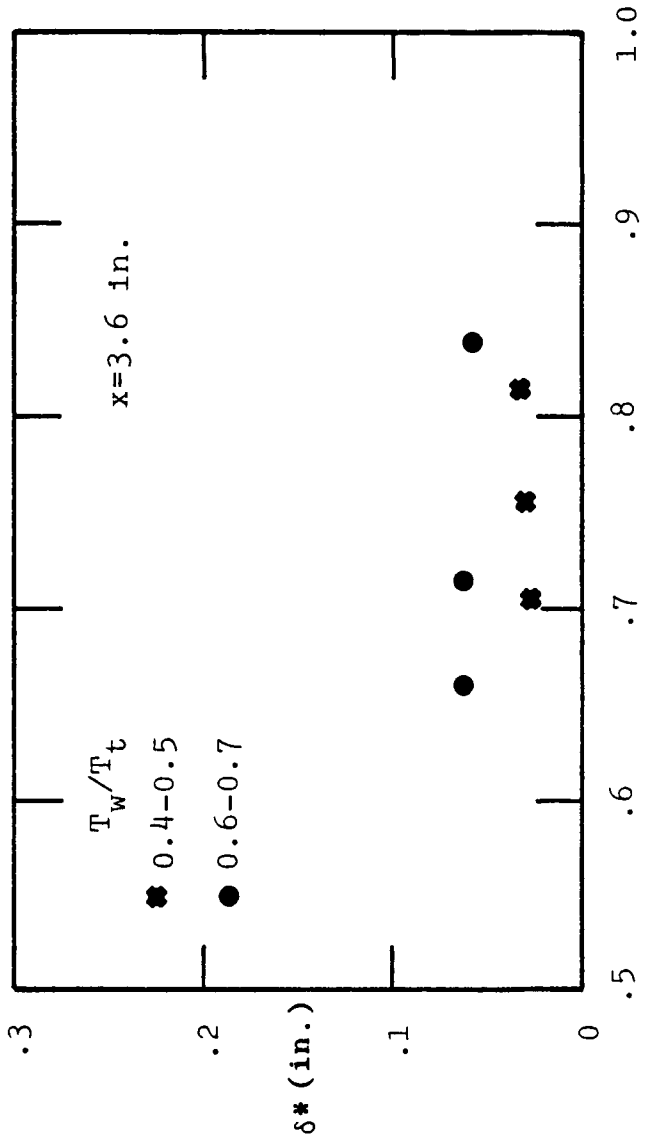


Figure 28. Displacement Thickness Downstream of Shock (Hot Run).

On the other hand, the displacement thicknesses δ^* calculated from wall static pressure measurement are shown in Figures 17-20, pages 35-38. The calculation procedure is given in Appendices D, E and F. δ^* is seen to grow in the downstream direction. δ^* just downstream of the shock is larger as the shock intensity becomes stronger. δ^* with cooling wall (⊠) is thinner than that without cooling (⊙), as expected. However, the difference of δ^* between the one with cooling and without cooling wall is small; this may be caused by one-dimensional flow treatment. In Figures 19 and 20, pages 37 and 38, the displacement thicknesses at $x = 3.6$ inches using the measured boundary layer profiles are plotted (● and ✖). These two kinds of data (⊙ vs. ● ; ⊠ vs. ✖) appear to agree qualitatively.

In Figures 12-14, pages 27-29, the length of the bifurcated oblique shocks with cooling wall are always shorter than the one without cooling wall. These phenomena again prove that the boundary layer thickness (or displacement thickness) with cooling wall just downstream of the shock for the same expansion ratio p_e/p_t are thinner than the one without cooling wall. The flow across the normal shock is subsonic, but the flow across the bifurcated oblique shock is supersonic [22]. Therefore, the mixing flow downstream of the shock without cooling wall becomes supersonic more rapidly than the one with cooling wall. With thinner boundary layer with cooling wall, a series

of normal shocks downstream of bifurcated normal shock becomes weak.

Figures 17-20 also contain the results of the boundary layer calculation downstream of the shock using Program STAN 5[2] Computer Code [23]; they are indicated by broken line (-----) for cooling and by chain line (— — —) for without cooling. For the low expansion ratio (Figure 20), the agreement between the experiment and calculation is satisfactory because the weak normal shock causes little, if any, flow separation. For the high expansion ratio (Figure 17), the strong normal shock separates the flow just downstream of the shock; such separated flow cannot adequately be dealt with by STAN 5. Hence the experimental data are higher than that of calculation.

As for the displacement thickness just upstream of the shock, because of the difficulty of measurement, no attempt is made for the present experiment. With regard to the calculated results, the values of δ^* estimated from

---

[2]STAN 5 Computer Code: The Navier-Stokes equations are solved using stream function. A large variety of two-dimensional flows can be accommodated by the program. The flow may be laminar or turbulent, and provision is made to handle transition. Fluid properties may be treated as constant or variable. The boundary conditions are involved injection and heat transfer. For turbulent flow, Prandtl mixing-length model and the turbulent kinetic energy model related to a velocity scale-length are included. The transformed equations are solved using finite-difference method.

Cline's[3] Computer Code [24] were 0.003 and 0.004 inch for wall with cooling and without cooling at $p_e/p_t \sim 0.7$, respectively. These results, showing that the boundary layer upstream of the shock is extremely thin, are consistent with the measured findings of Figure 11, page 26, where the pressure distribution remains the same both for a wall with and without cooling. Note, however, that $\delta^* = 0.003$ for the wall with cooling is again smaller than $\delta^* = 0.004$ for the one without cooling.

5. Shift of Normal Shock

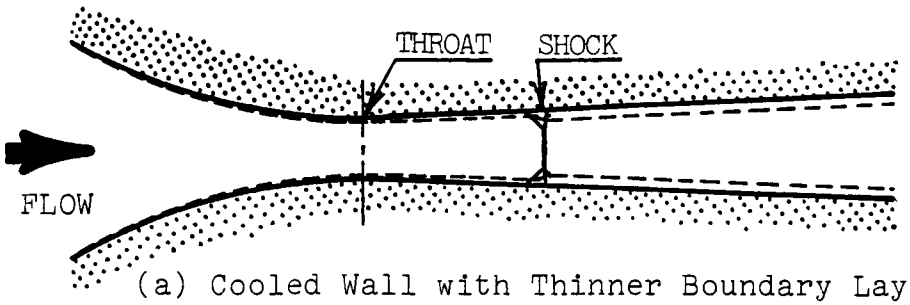
As seen in Figures 12-15, pages 27-30, for the hot run, the wall cooling shifts the position of the normal shock in the downstream direction. The shift becomes large for the low expansion ratio (Figure 12) and becomes small for the high expansion ratio (Figure 15). As mentioned previously, for hot run, the displacement thickness downstream of the shock between the one with cooling and without cooling is sizeable; δ^* for the cooled wall is about one-half of the δ^* for the wall without cooling (Figure 18). This difference in δ^* effectively alters the

---

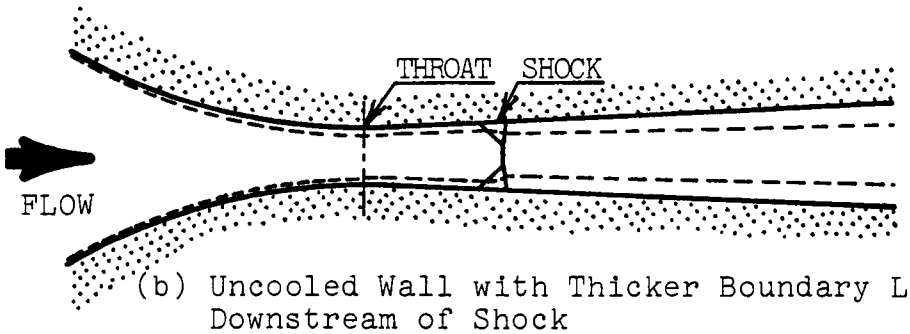
[3]Cline's Computer Code: The Navier-Stokes equations for two-dimensional, time-dependent and compressible flow are solved using the second-order accurate finite difference method. The boundary mesh points are calculated using a characteristic scheme with the viscous terms treated as source functions. A mixing-length model is included for turbulent flows. The steady-state condition is obtained as the asymptotic solution for large time.

cross-sectional area of flow and hence changes the blockage, which in turn causes the shift in the shock position; the details of this are now discussed by referring to Figure 29.

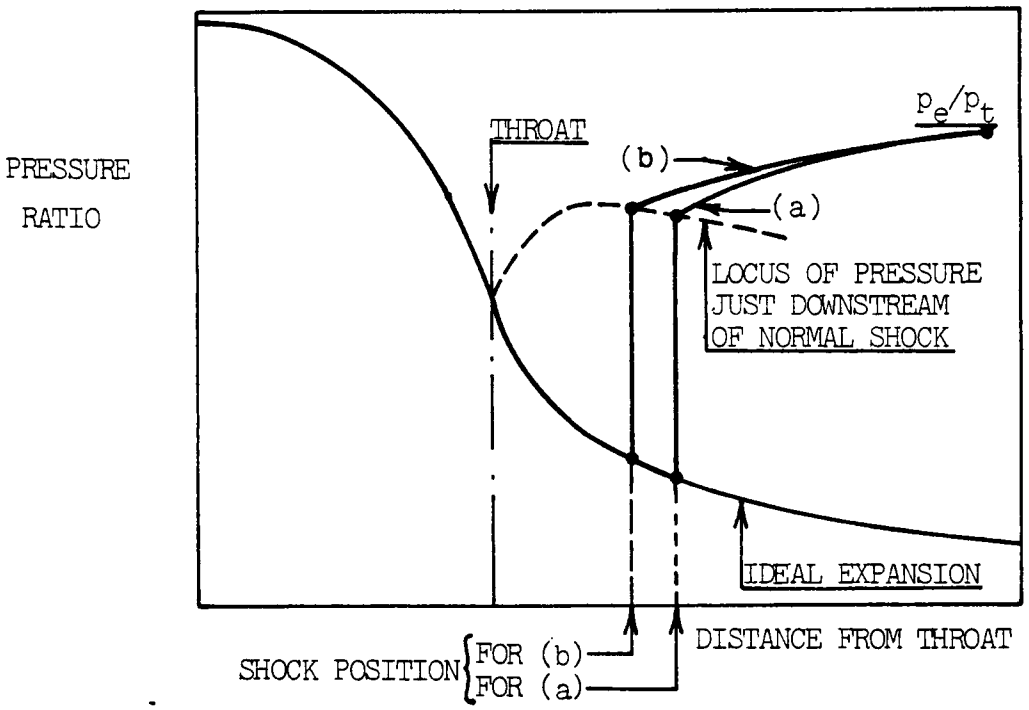
Figure 29 displays the effects of the boundary layer thickness schematically. The boundary layer develops in a different manner, depending upon the wall condition, i.e., whether it is cooled or uncooled. Especially in the region downstream of the shock, the diffusion--the degree of flow expansion--for the uncooled wall (Figure 29(b)) is less than the one for the cooled wall (Figure 29(a)). Consequently, for the same expansion ratio p_e/p_t , the pressure distribution downstream of the shock differs in the manner indicated by (a) and (b), as shown in Figure 29(c). With respect to the region upstream of the shock, when one adds the pressure rise across a normal shock to the ideally expanded pressure, the locus of pressure just downstream of normal shock is obtained; the intersect of this with the pressure distribution of the subsonic diffuser part determines the shock position. Thus, it is seen that the position of the shock for the cooled wall is shifted in the downstream direction; this explains the reason for such a shift due to cooling. When the shock approaches the throat, the pressure rise across the shock becomes reduced; the shock becomes so weak that the difference in the displacement thickness tends



(a) Cooled Wall with Thinner Boundary Layer Downstream of Shock



(b) Uncooled Wall with Thicker Boundary Layer Downstream of Shock



(c) Shift in Shock Position

Figure 29. Effect of Cooling upon Boundary Layer Thickness Downstream of Shock.

to disappear; thus the shift in the shock position becomes less as the expansion ratio p_e/p_t is increased and this agrees with the trend observed in Figure 15.

CHAPTER VI

CONCLUSIONS

The present study has experimentally examined the interaction of heat transfer in the two-dimensional convergent-divergent duct representative of a turbine passage; the main objective is to investigate the effect of cooling on the transonic flow field. The experiment was carried out in the following range of parameters: $p_t \simeq 4$-20 psig, $T_t \simeq 40 \sim 1000°F$ and $T_w \simeq 50$-$900°F$. From this experiment the following conclusions have been drawn:

1. It was confirmed that the change of the sonic location due to the heat transfer was small in the present experimental conditions.

2. The flow in the duct was always turbulent throughout the experiments. The velocity profiles upstream and downstream of the shock agree favorably with the "law of the wall."

3. The displacement thicknesses downstream of the shock were 0.061 inch for a wall without cooling and 0.031 inch for a wall with cooling at the position of 3.6 inches downstream of the throat. These values were almost the same regardless of the shock location.

4. The lengths of the bifurcated oblique shocks with cooling wall were shorter than the one without cooling wall, and the displacement thickness with cooling wall

became thin. With thinner boundary layer with cooling wall, a series of normal shocks downstream of bifurcated normal shock became weak.

5. The position of the shock was shifted by the effect of wall cooling. For $T_w/T_t \sim 0.5$ and $p_e/p_t \sim 0.5$, not untypical values for the transonic stator, the amount of the shock movement was found to be of the same order as the throat height; the physical explanation for this shift has been offered.

LIST OF REFERENCES

LIST OF REFERENCES

1. McDonald, P. W. "The Computation of Transonic Flow through Two-Dimensional Gas Turbine Cascades," The American Society of Mechanical Engineers Paper No. '71-GT-89, 1971.

2. Delaney, R. A., and P. Kavanaugh. "Transonic Flow Analysis in Axial-Flow Turbomachinery Cascades by a Time-Dependent Method of Characteristics," Transactions of the ASME, Series A, Journal of Engineering for Power, Vol. 98, No. 3, 1976, pp. 356-364.

3. Ives, D. C., and J. F. Luitermoza. "Analysis of Transonic Cascade Flow Using Conformal Mapping and Relaxation Techniques," AIAA Journal, Vol. 15, No. 5, 1977, pp. 647-652.

4. Gliebe, P. R. "Coupled Inviscid/Boundary-Layer Flow Field Predictions for Transonic Turbomachinery Cascades," Transonic Flow Problems in Turbomachinery, edited by Adamson, T. C., Jr., and M. F. Platzer, Washington D.C.: Hemisphere Publishing Corporation, 1976, pp. 434-453.

5. Hartsel, J. E. "Prediction of Effects of Mass-Transfer Cooling on the Blade-Row Efficiency of Turbine Airfoils," The American Society of Mechanical Engineers Paper 72-11, 1972.

6. Whitney, Warren J., E. M. Szanca, and D. E. Monroe. "Cold Air Investigation of a Turbine for High Temperature Engine Application, I: Turbine Design and Overall Stator Performance," National Aeronautics and Space Administration, Technical Note D-3751, Washington D.C., 1967.

7. Prust, Herman W., H. J. Schum and F. P. Behning. "Cold Air Investigation of a Turbine for High-Temperature Engine Application, II. Detailed Analytical and Experimental Investigation of Stator Performance," National Aeronautics and Space Administration, Technical Note D-4418, Washington, D.C., 1968.

8. Whitney, W. J., E. M. Szanca and F. P. Behning. "Cold Air Investigation of a Turbine with Stator-Blade Trailing-Edge Coolant Injection, I. Overall Stator Performance," National Aeronautics and Space Administration, Technical Memorandum X-1901, Washington, D.C., 1969.

9. Prust, H. W., H. J. Schum and E. M. Szanca. "Cold Air Investigation of a Turbine with Transpiration-Cooled Stator Blades, I. Performance of Stator with Discrete Hole Blading," National Aeronautics and Space Administration, Technical Memorandum X-2094, Washington, D.C., 1970.

10. Behning, F. P., H. W. Prust and T. P. Moffitt. "Cold Air Investigation of a Turbine with Transpiration-Cooled Stator Blades, III. Performance of Stator Blades with Wire-Mesh Shell Blading," National Aeronautics and Space Administration, Technical Memorandum X-2166, Washington, D.C., 1971.

11. Shapiro, Ascher H. The Dynamics and Thermodynamics of Compressible Fluid Flow, Vol. 1, New York, Ronald Press, 1953. p. 231.

12. Studerus, C. J. "Aerodynamic Effects of Surface Cooling-Flow Injection on Turbine Transonic Flow Fields," American Institute of Aeronautics and Astronautics Paper No. 79-0048, presented at AIAA 17th Aerospace Sciences Meeting, New Orleans, Louisiana, 1979.

13. Kurosaka, M., H. P. Chou, H. Kuroda and J. M. Wu. "Aerodynamic Interaction of Heat Transfer with Steady Transonic Flow," American Institute of Aeronautics and Astronautics Paper No. 81-0275, presented at AIAA 19th Aerospace Sciences Meeting, St. Louis, Missouri, 1981.

14. Shapiro, Ascher H. The Dynamics and Thermodynamics of Compressible Fluid Flow, Vol. 1, New York, Ronald Press, 1953, p. 258.

15. Patel, V. C., and M. R. Head. "Reversion of Turbulent to Laminar Flow," Journal of Fluid Mechanics, Vol. 34, Part 2, 1968, pp. 371-392.

16. Boldman, D. R., J. F. Schmidt and A. K. Gallagher. "Laminarization of a Turbulent Boundary Layer as Observed from Heat Transfer and Boundary Layer Measurements in Conical Nozzles," National Aeronautics and Space Administration, Technical Note D-4788, Washington, D.C., 1968.

17. Boldman, D. R., and R. W. Graham. "Heat Transfer and Thermal Boundary Layer in a Conical Nozzle," American Institute of Aeronautics and Astronautics Paper No. 69-474, presented at AIAA 5th Propulaion Joint Specialist Conference, U.S. Air Force Academy, Colorado, 1969.

18. Back, L. H., R. F. Cuffel and P. F. Massier. "Laminarization of a Turbulent Boundary Layer in Nozzle-Flow, Boundary Layer and Heat Transfer Measurement with Wall Cooling," Transactions of the ASME, Series C, Journal of Heat Transfer, August 1970, pp. 333-344.

19. Mager, Artur. "Prediction of Shock-Induced Turbulent Boundary Layer Separation," Journal of Aeronautical Sciences, Vol. 22, No. 3, 1955, pp. 201-202.

20. Mager, Artur. "On the Model of the Free, Shock-Separated, Turbulent Boundary Layer," Journal of Aeronautical Sciences, Vol. 23, No. 2, 1956, pp. 181-184.

21. Sehgal, R., and J. M. Wu. "Thrust Vector Control by Liquid Injection into Rocket Nozzles," Journal of Spacecraft and Rockets, Vol. 1, No. 5, 1964, pp. 545-551.

22. Sedden, J. "The Flow Produced by Interaction of a Turbulent Boundary Layer with a Normal Shock Wave of Strength Sufficient to Cause Separation," Aeronautical Research Council, Reports and Memoranda No. 3502, London, 1967.

23. Crawford, M. E., and W. M. Kays. "STAN 5," "A Program for Numerical Computation of Two-Dimensional Internal and External Boundary Layer Flows," National Aeronautics and Space Administration, Contract Report No. 2742, Washington, D.C., 1976.

24. Cline, M.C. "VNAP," "A Computer Program for Computation of Two-Dimensional, Time-Dependent Compressible, Viscous Internal Flow," Los Alamos Scientific Laboratory Report LA-7326, California: University of California, 1978.

25. Schlichting, H. Boundary Layer Theory, 7th Edition, New York: McGraw-Hill Book Co., 1979, p. 471 and pp. 702-728.

26. Liepmann, H. W., and A. Roshko. Elements of Gasdynamics, New York: John Wiley & Sons, Inc., 1957, pp. 147-149.

27. White, Frank M. Viscous Fluid Flow, New York: McGraw-Hill Book Co., 1974, pp. 586-600.

APPENDICES

APPENDIX A

RELATIONSHIP BETWEEN HEAT TRANSFER AND SHIFT OF SONIC LINE

The heat transfer per unit mass Q is related to the wall heat flux per unit area q_w . In the present experiment, the contour of convergent-divergent duct is given by

$$\frac{h}{2} = 10\left\{1 - \cos\left[\sin^{-1}\frac{x}{10}\right]\right\} + 0.45 \qquad \text{for } -7 \leq x \leq 0.46 \quad , \tag{A.1}$$

$$\frac{h}{2} = (x - 0.46)\tan\left[2.62\,\frac{\pi}{180}\right] + 0.46 \qquad \text{for } 0.46 \leq x \leq 12 \, , \tag{A.2}$$

$$\frac{h_{th}}{2} = 0.45 \qquad \text{at throat } (x = 0) \quad . \tag{A.3}$$

Consider the flow in a duct between two sections separated by an infinitesimal distance dx . If the span of duct is 8 inches, then

$$3600 \cdot G \cdot dQ = 2 \cdot q_w \cdot \frac{8}{12} \cdot \frac{dx}{12} \quad . \tag{A.4}$$

The heat transfer per unit mass is given by

$$\frac{dQ}{c_p T} = 3.086 \times 10^{-5}\,\frac{q_w}{c_p T}\,\frac{dx}{G} \quad . \tag{A.5}$$

The shift of sonic line is given by [14]

$$\frac{dA}{A} = \frac{dQ}{c_p T} \quad . \tag{A.6}$$

From equation (A.1),

$$\frac{dA}{A} = \frac{dh}{h} = \frac{\frac{x}{10}}{\sqrt{1-\left(\frac{x}{10}\right)^2}} \frac{dx}{10\left\{1-\cos\left(\sin^{-1}\frac{x}{10}\right)\right\}+0.45} \quad . \tag{A.7}$$

Thus, the relationship between the sonic line position and the heat transfer is given by:

$$\frac{\frac{x}{10}}{\sqrt{1-\left(\frac{x}{10}\right)^2}} \frac{1}{10\left\{1-\cos\left(\sin^{-1}\frac{x}{10}\right)\right\}+0.45} = 3.086\times10^{-5}\frac{q_w}{c_p T}\frac{1}{G} \quad . \tag{A.8}$$

The range of the parameters used in the present experiment was

$$\left.\begin{array}{rll} -2\times10^4 \leq q_w \leq 1\times10^4 & \text{Btu/ft} \\ 1 \leq G \leq 6.3 & \text{lbm/sec} \\ 500 \leq T \leq 1500 & {}^\circ\text{R} \end{array}\right\} \quad . \tag{A.9}$$

Then the shift of sonic line was

$$-0.02 \leq x \leq 0.01 \text{ inches} \quad . \tag{A.10}$$

APPENDIX B

ACCELERATION PARAMETER

The critical acceleration parameter for an axisymmetric flow was derived from the integral momentum equation in Reference [16]. Here, we derive its counterpart applicable to two-dimensional flow. The integral momentum equation for two-dimensional flow is given by

$$\frac{d\theta}{dx} + \left(\frac{2+H}{u_e}\frac{du_e}{dx} + \frac{1}{\rho_e}\frac{d\rho_e}{dx}\right)\theta = \frac{\tau_w}{\rho_e u_e^2} \quad , \tag{B.1}$$

where the form factor $H = \delta^*/\theta$ may be regarded as the function of a pressure-gradient parameter. Equation (B.1) can be rewritten as

$$\frac{d\,Re_\theta}{dx} = \frac{\rho_e u_e}{\mu_e}\left(\frac{\tau_w}{\rho_e u_e^2} - K \cdot Re_\theta(1+H)\right) \quad , \tag{B.2}$$

where $Re_\theta = \rho_e u_e \theta/\mu_e$ is the Reynolds number based on momentum thickness and the dynamic viscosity μ_e is assumed constant, and

$$K = \frac{\mu_e}{\rho_e u_e^2}\frac{d\,u_e}{dx} \quad . \tag{B.3}$$

In order for relaminarization to occur, the value of $d\,Re_\theta/dx$ must be equal to zero or negative at the critical Reynolds number of Re_θ . The critical

Reynolds number based on displacement thickness and the wall shearing stress over the flat plate are given by [25]:

$$Re_{\delta^*} = 950 \quad , \tag{B.4}$$

$$\frac{\tau_w}{\rho_e u_e^2} = 0.0225 \left(\frac{\mu_e}{\rho_e u_e \delta} \right)^{1/4} = 0.0134 \, Re_{\delta^*}^{-1/4} \quad , \tag{B.5}$$

respectively. Therefore, the following inequality has to be satisfied, by assuming H = 1.29 [25]:

$$K > \frac{1}{Re_\theta (1 + H)} \frac{\tau_w}{\rho_e u_e^2} \simeq 1.4 \times 10^{-6} \quad . \tag{B.6}$$

APPENDIX C

WALL HEAT FLUX FROM TOP AND BOTTOM WALLS

Taking the y-axis perpendicular to the wall, the basic Fourier equation for the wall heat flux is given by:

$$q_w = - k_w \left.\frac{\partial T_b}{\partial y}\right|_{y = 0} \quad . \tag{C.1}$$

The temperature distribution is given by the equation (D.7); therefore

$$\left.\frac{\partial T_b}{\partial y}\right|_{y = 0} = \frac{T_e}{M_e} \sqrt{\frac{T_w}{T_e}} \left(1 + r \frac{\gamma - 1}{2} M_e - \frac{T_w}{T_e}\right) \left.\frac{\partial M_b}{\partial y}\right|_{y = 0} \quad . \tag{C.2}$$

Near the wall, velocity profile from the "law of the wall" can be expressed by:

$$u^+ = y^+ \qquad \text{or} \qquad M_b a_b = \frac{\rho_w u_\tau^2}{\mu_w} y \quad . \tag{C.3}$$

The derivative of equation (C.3) with respect to y is given by:

$$\left.\frac{\partial M_b}{\partial y}\right|_{y = 0} = \frac{\rho_w u_\tau^2}{a_w \mu_w} \quad . \tag{C.4}$$

Therefore the wall heat flux turns into

$$q_w = - \frac{\rho_w c_p T_e u_\tau^2}{Pr_w} \left(1 + r \frac{\gamma - 1}{2} M_e^2 - \frac{T_w}{T_e} \right) , \qquad (C.5)$$

where Pr is Prandtl number.

APPENDIX D

DATA REDUCTION WITHIN BOUNDARY LAYER

The velocity within the boundary layer changes from subsonic to supersonic flow. The Mach number is evaluated from pitot pressure measurement in flow by the following approaches.

When the flow is subsonic, the pitot pressure is the true total pressure. Mach number is, therefore, obtained from the following isentropic relationship:

$$M_b = \left\{ \frac{2}{\gamma - 1} \left[\frac{1}{\left(\frac{p}{p_{t,b}} \right)^{\frac{\gamma-1}{\gamma}}} - 1 \right] \right\}^{1/2} . \qquad (D.1)$$

When the flow is supersonic, a detached shock will be generated ahead of a pitot probe. The detached shock wave is locally normal to the stagnation streamline. The total pressure downstream of the detached shock is indicated as pitot total pressure. The Mach number upstream of the detached shock can be obtained by applying the normal shock relationship; it is the so-called Rayleigh supersonic pitot formula [26], given by:

$$M_b = \left\{ \left(\frac{2}{\gamma + 1} \right)^{\gamma+1} \left(\frac{p_{t,b}}{p} \right)^{\gamma-1} \left(\gamma M_b^{\,2} - \frac{\gamma - 1}{2} \right) \right\}^{1/2\gamma} . \qquad (D.2)$$

It is convenient to use the displacement thickness instead of the boundary layer thickness. The displacement thickness is a measure of the deficiency in mass flow through the boundary layer as a result of the flow being slowed down by friction. Displacement thickness can be defined by

$$\delta^* \equiv \int_0^{h/2} \left(1 - \frac{\rho}{\rho_e} \frac{u}{u_e}\right) dy = \int_0^{h/2} \left(1 - \frac{M_b}{M_e} \frac{a_e}{a_b}\right) dy \quad , \qquad (D.3)$$

where the static pressure through the boundary layer is assumed constant.

Though the edge of the displacement thickness is not streamline, even when the actual walls are displaced by the amount corresponding corresponding to the displacement thickness, the flow outside would remain the same if it were inviscid. The displacement thickness can be predicted in two ways by using either boundary layer velocity distribution or wall static pressure distribution.

In the former case, it is necessary to obtain the acoustic speed in equation (D.3) which is the function of temperature. The temperature profile is derived by applying Crocco-Busemann approximation [27], which is applicable to turbulent flow.

$$\frac{T_b}{T_e} = \frac{T_w}{T_e} + \left(1 + r \frac{\gamma - 1}{2} M_e^2 - \frac{T_w}{T_e}\right) \frac{u_b}{u_e} - r \frac{\gamma - 1}{2} M_e^2 \left(\frac{u_b}{u_e}\right)^2 \quad . \qquad (D.4)$$

Since

$$\frac{T_b}{T_e} = \left(\frac{a_b}{a_e}\right)^2 \quad , \quad \frac{u_b}{u_e} = \frac{M_b}{M_e} \cdot \frac{a_b}{a_e} \quad , \tag{D.5}$$

(D.4) will become a quadratic equation for a_b/a_e . Then the acoustic speed and additional temperature become

$$\frac{a_b}{a_e} = \frac{1}{2B_o}\left\{A_o + \left(A_o^2 + 4B_o \frac{T_w}{T_e}\right)^{1/2}\right\} \quad , \tag{D.6}$$

$$\frac{T_b}{T_e} = \frac{1}{B_o}\frac{T_w}{T_e} + \frac{A}{2B_o^2}\left\{A_o + \left(A_o^2 + 4B_o \frac{T_w}{T_e}\right)^{1/2}\right\} \quad , \tag{D.7}$$

where

$$A_o = \left(1 + r\frac{\gamma - 1}{2}M_e^2 - \frac{T_w}{T_e}\right)\frac{M_b}{M_e} \quad , \quad B_o = 1 + r\frac{\gamma - 1}{2}M_b^2 \quad . \tag{D.8}$$

In the latter case, the pressure ratio will give the area ratio if one adopts the one-dimensional treatment [14]. The boundary layer will develop not only on the top and bottom walls but also on the sidewalls. It is assumed that the displacement thickness on the sidewalls takes the same value as that of top or bottom wall. Since the span of the present convergent-divergent duct is 8 inches, the area ratio can be written by:

$$\frac{A}{A_{th}} \simeq \frac{8h - 2\delta^{*}\ (8 + h)}{8h_{th} - 2\delta^{*}_{th}\left(8 + h_{th}\right)} \quad . \tag{D.9}$$

Then the displacement thickness can be expressed by:

$$\delta^{*} = \frac{\frac{h}{2} - \frac{A}{A_{th}} \left\{\frac{h_{th}}{2} - \delta^{*}_{th} \left[1 + \frac{1}{4} \cdot \frac{h_{th}}{2}\right]\right\}}{1 + \frac{1}{4}\,\frac{h}{2}} \quad . \tag{D.10}$$

In the present experiment, it is expected that the displacement thickness at the throat is small ($\delta^{*}_{th}/h_{th} \sim 0.015$). Therefore, if δ^{*}_{th} is neglected, equation (D.10) will become

$$\delta^{*} = \frac{\frac{h}{2} - \frac{A}{A_{th}}\,\frac{h_{th}}{2}}{1 + \frac{1}{4}\,\frac{h}{2}} \quad . \tag{D.11}$$

APPENDIX E

PRESSURE RATIO AND MACH NUMBER UPSTREAM OF SHOCK

In data reduction process the flow is assumed to be steady, one-dimensional, that gas properties are function of temperature only and obey perfect gas rules. Equation of state, acoustic speed and equation of continuity are:

$$p = \rho RT \quad , \tag{E.1}$$

$$a^2 = \gamma RT = \frac{\gamma p}{\rho} \quad , \tag{E.2}$$

$$G = \rho u A \quad . \tag{E.3}$$

Heat transfer rate Q transferred from top and bottom walls is given by:

$$Q = c_p\left(T_t - T_{t,ref}\right) \quad , \tag{E.4}$$

where $T_{t,ref}$ is the reference total temperature. In the present experiment, the settling total temperature $T_{t,st}$ is chosen. Since the variation of specific heat c_p is small in the present case, it may be neglected.

Hence,

$$c_p = \text{const} = \frac{\gamma}{\gamma - 1} R \quad . \tag{E.5}$$

The stagnation or total temperature and pressure may be expressed as

$$T_t = T\left(1 + \frac{\gamma - 1}{2} M^2\right) \quad , \tag{E.6}$$

$$p_t = p\left(1 + \frac{\gamma - 1}{2} M^2\right)^{\frac{\gamma}{\gamma-1}} \quad . \tag{E.7}$$

From equations (E.4) and (E.6), the total temperature ratio is obtained as:

$$\frac{T_{t,st}}{T_{t,th}} = 1 - \frac{\left(\frac{Q}{c_p T}\right)_{th}}{1 + \frac{\gamma - 1}{2} M_{th}^2} \quad . \tag{E.8}$$

For the present test section, using equation (A.5) turns out to be

$$-\left(\frac{Q}{c_p T}\right)_{th} \sim 0.012 \quad . \tag{E.9}$$

Thus, the difference in the total temperatures between settling chamber and throat is only 1.2%. Also, as shown in Appendix A, the sonic line corresponding to the present situation is still located near the throat, even in the presence of heat transfer; therefore, it may be assumed as a good approximation that the flow upstream of the shock is isentropic. The so-called critical pressure ratio occurring at the throat is given by:

$$\frac{p_{th}}{p_t} = \left(\frac{2}{\gamma + 1}\right)^{\frac{\gamma}{\gamma-1}} \quad . \tag{E.10}$$

After some reduction, the relationship between area and pressure and the one between Mach number and pressure can be rewritten, respectively, as

$$\left(\frac{A}{A_{th}}\right)^2 = \frac{\frac{\gamma - 1}{2}\left(\frac{2}{\gamma + 1}\right)^{(\gamma+1)/(\gamma-1)}}{\left(\frac{p}{p_t}\right)^{2/\gamma} - \left(\frac{p}{p_t}\right)^{(\gamma+1)/\gamma}} \quad , \tag{E.11}$$

$$M^2 = \frac{2}{\gamma - 1}\left\{\frac{1}{\left(\frac{p}{p_t}\right)^{(\gamma-1)/\gamma}} - 1\right\} \quad . \tag{E.12}$$

APPENDIX F

AREA RATIO DOWNSTREAM OF SHOCK

The behavior of the normal shock within a duct is complex. The locations of shock are influenced by the separation of the boundary layer near the shock legs as well as the shock and boundary layer interaction which, in turn, induces a set of secondary shocks. Both of them contribute to the thickening of displacement thickness, which changes the effective cross-sectional area of the duct.

To simplify the data reduction procedure, we assume, first, that only a single normal shock exists. The relationships across the normal shock are

$$M_2^2 = \frac{1 + \frac{\gamma - 1}{2} M_1^2}{M_1^2 - \frac{\gamma - 1}{2}} \quad , \tag{F.1}$$

$$\frac{p_2}{p_1} = \frac{1 + \gamma M_1^2}{1 + \gamma M_2^2} \quad . \tag{F.2}$$

The area and Mach number just upstream of the normal shock can be derived by

$$\left(\frac{A_1}{A_{th}}\right)^2 = \frac{\frac{\gamma - 1}{2} \left(\frac{2}{\gamma + 1}\right)^{(\gamma+1)/(\gamma-1)}}{\left(\frac{p_1}{p_t}\right)^{2/\gamma} - \left(\frac{p_1}{p_t}\right)^{(\gamma+1)/\gamma}} \quad , \tag{F.3}$$

$$M_1^2 = \frac{2}{\gamma - 1} \left\{ \frac{1}{\left(\frac{p_1}{p_t}\right)^{(\gamma-1)/\gamma}} - 1 \right\} \quad . \tag{F.4}$$

The ratio of total pressure across the normal shock is

$$\frac{p_{t,2}}{p_{t,1}} = \frac{2}{\gamma - 1} \left(\frac{\gamma + 1}{2}\right)^{\frac{\gamma+1}{\gamma-1}} \left(\frac{p_1}{p_{t,1}}\right)^{\frac{1}{\gamma}} \left[\frac{\left\{ 1 + \left(\frac{p_1}{p_{t,1}}\right)^{\frac{\gamma-1}{\gamma}} \right\}^{\gamma}}{\gamma - \left(\frac{\gamma + 1}{2}\right)^2 \left(\frac{p_1}{p_{t,1}}\right)^{\frac{\gamma-1}{\gamma}}} \right]^{\frac{1}{\gamma-1}} \quad . \tag{F.5}$$

Therefore, the area ratio may be written by

$$\frac{A}{A_{th}} = \frac{A_1}{A_{th}} \cdot \frac{M_2}{M} \cdot \left(\frac{p_2}{p_1}\right)^{\frac{\gamma-1}{2\gamma}} \left(\frac{\frac{p_1}{p_{t,1}}}{\frac{p}{p_{t,1}}} \right)^{\frac{\gamma-1}{2\gamma}} \quad . \tag{F.6}$$

VITA

Hiromoto Kuroda was born on February 11, 1942, in Shobara-City, Hiroshima, Japan.

In April 1961 he entered the Science University of Tokyo and received his Bachelor of Science degree in Physics in March 1965.

He has been employed by The National Defense Academy of Japan in the Department of Aeronautical Engineering since April 1965. He took the postgraduate course on Aerospace Vehicle Engineering at The National Defense Academy during April 1967 and March 1969.

He accepted a Research Assistantship from The University of Tennessee Space Institute and started his graduate education in Engineering Science and Mechanics in September 1979.

Mr. Kuroda is a member of The Japan Society of Mechanical Engineers, Japan Society for Aeronautical and Space Sciences, The Gas Turbine Society of Japan, and Heat Transfer Society of Japan. He is a student member of the American Institute of Aeronautics and Astronautics, and a member of Sigma Chi.

He is married to the former Yasuko Horie of Shobara-City, Hiroshima, Japan, and has two sons, Akihiro and Nobuhiro.